The roles of toughness and cohesive strength on crack deflection at interfaces

J. P. Parmigiani[1*] and M. D. Thouless[1,2]
[1]*Department of Mechanical Engineering*
[2]*Department of Materials Science & Engineering*
University of Michigan
Ann Arbor, MI 48109

August 30, 2005

Abstract

In order to design composites and laminated materials, it is necessary to understand the issues that govern crack deflection and crack penetration at interfaces. Historically, models of crack deflection have been developed using either a strength-based or an energy-based fracture criterion. However, in general, crack propagation depends on both strength and toughness. Therefore, in this paper, crack deflection has been studied using a cohesive-zone model which incorporates both strength and toughness parameters simultaneously. Under appropriate limiting conditions, this model reproduces earlier results that were based on either strength or energy considerations alone. However, the general model reveals a number of interesting results. Of particular note is the apparent absence of any lower bound for the ratio of the substrate to interface toughness to guarantee crack penetration. It appears that, no matter how tough an interface is, crack deflection can always be induced if the strength of the interface is low enough compared to the strength of the substrate. This may be of significance for biological applications where brittle organic matrices can be bonded by relatively tough organic layers. Conversely, it appears that there is a lower bound for the ratio of the substrate strength to interfacial strength, below which penetration is guaranteed no matter how brittle the interface. Finally, it is noted that the effect of modulus mismatch on crack deflection is very sensitive to the mixed-mode failure criterion for the interface, particularly if the cracked layer is much stiffer than the substrate.

*Current address: Department of Mechanical Engineering, Oregon State University, Corvallis, OR 97331

1 Introduction

1.1 Contribution of crack deflection to toughening

Crack deflection and delamination at interfaces play a major role in the performance of many composite systems. Brittle materials such as ceramics, concrete or epoxies can be toughened by the addition of relatively brittle fibers, provided crack deflection occurs at the interfaces between the fibers and the matrix. If crack deflection does not occur, a crack propagating through the matrix will continue unimpeded when it encounters the fiber. This results in little or no toughening, as relatively little energy is dissipated by fracture of a brittle fiber. Conversely, if crack deflection does occur, then the crack is effectively blunted. Furthermore, if the crack circumvents the fibers and continues to propagate without penetrating them, the intact fibers left behind in the crack wake bridge the crack surfaces (Fig. 1a). Significant contributions to toughening can then be provided by energy that is dissipated by friction at the debonded fiber-matrix interfaces [1, 2, 3, 4]. Similar effects occur during the fracture of composites reinforced by whiskers or particles [5, 6, 7], or of polycrystalline materials [8, 9]. Deflection along interfaces in these materials results in toughening by crack bridging, frictional pull-out, or crack deflection [10, 11] (Fig. 1b).

Laminated composites provide another class of engineering materials for which crack deflection at interfaces plays a crucial role in their mechanical properties [12, 13, 14, 15, 16] (Fig. 1c). Deflection along multiple interlaminar interfaces results in dissipation of energy by the delamination process. In addition, cracks often need to be re-initiated in undamaged plies in such materials; this process also contributes to the strength of the composite. Deflection of cracks along the interfaces in single and multilayer coatings (Fig. 1d) provides the same mechanism for protecting substrates, which is of particular use in wear applications [17, 18].

Many natural materials are composites, and rely upon crack deflection to provide exceptional levels of toughness [19, 20, 21, 22]. For example, wood consists of aligned long, hollow cylindrical cells [23, 24], and common experience shows that attempts to fracture wood perpendicular to its grain are hindered by crack deflection along the grains. Shells of many animals provide examples of materials with exceptional toughness created by combining a hard, brittle, inorganic mineral with a compliant protein [25]. The protein exists at the interfaces between the mineral components, and provides a bonding agent that can delaminate and dissipate energy when an attempt is made to fracture the shell. It is clear that the balance between the organic interface and inorganic matrix is highly optimized for the evolutionary purposes of the shell.

1.2 Previous analyses of crack deflection

The optimization of composites that exhibit crack deflection and interfacial delamination requires an understanding of how the interfacial and bulk properties affect the mechanics of the problem. The role of crack deflection at interfaces was first recognized and analyzed about forty years ago by Cook and Gordon [26]. Their analysis used a strength-based fracture criterion. They considered a matrix crack perpendicular to a fiber having identical elastic properties as the matrix. The matrix crack was modeled as an ellipse with a very high aspect ratio, and the results of Inglis [27] were used to investigate the stresses around the crack tip. Cook and Gordon [26] noted that the maximum normal stress ahead of, and co-planar with, the crack is about five times greater than the maximum normal stress perpendicular to the crack tip. Based on this observation, they suggested that a fiber needs to be about five times stronger than the interface between it and the matrix to prevent fiber fracture, and to allow crack deflection to occur.

This concept was extended many years later by Gupta *et al.* [28], who used earlier work [29, 30, 31] on the stress field around a sharp crack at bimaterial interfaces, to look at the criterion for determining whether a crack at normal incidence to a bimaterial interface would deflect or not. Comparisons between the maximum normal stress across the interface and the maximum normal stress ahead of the crack allowed predictions to be made about whether deflection or penetration should occur. For example, in an elastically homogeneous system, the results indicated that crack deflection should occur if the material ahead of the crack is more than about three and a half times stronger than the interface. While giving a slightly different value for the ratio of the two strengths required for deflection, this result is consistent with the earlier work of Cook and Gordon [26]. Furthermore, this work showed that crack deflection along the interface becomes much less likely if the cracked matrix is stiffer than the second phase, with crack deflection becoming essentially impossible if there is a compliant second phase embedded in a rigid matrix. Conversely, the tendency for crack deflection increases slightly when the second phase is stiffer than the matrix.

These analyses follow an Inglis [27] or strength-based approach to fracture. Both analyses lead to design criteria for composites and laminates that are based on the ratio of the strengths of the interface and second phase. An alternative approach using interfacial fracture mechanics [32] follows that of Griffith [33] and others [34, 35, 36], and is based on an energy criterion. Many authors have used linear-elastic fracture mechanics to look at crack deflection from an energy perspective [37, 38, 39, 40, 41, 42]. These generally follow the approach of Cotterell and Rice [43], where the energy-release rates of kinks at different angles ahead of a main crack are considered. The ratio of the energy-release rates in different directions is taken to be proportional to the critical ratio of the toughnesses required to trigger fracture in the different directions.

Of particular note is the work by He and Hutchinson [37], with corrections [40, 39]. In their work, the problem of determining whether crack deflection or penetration occurs when a crack impinges a bimaterial interface in a normal direction was examined by comparing the energy-release rate at the tip of a small kink extending across the interface, $\mathcal{G}_p$, with the energy-release rate at the tip of a small kink deflected along the interface, $\mathcal{G}_d$ (Fig. 2). The condition for crack deflection along the interface can be written as

$$\frac{\Gamma_i}{\Gamma_s} < \frac{\mathcal{G}_d}{\mathcal{G}_p}, \tag{1}$$

where Γ_i is the toughness of the interface under the appropriate mixed-mode conditions, and Γ_s is the toughness of the material (substrate) ahead of the interface. One particularly well-known result is that when the elastic properties across the interface are identical, and the kinks are vanishingly small, crack deflection occurs if the toughness of the material on the other side of the interface is more than approximately four times the mixed-mode toughness of the interface [37, 38].

1.3 Problem addressed in the present work

In the analyses described above, two different fracture criteria were used: a stress-based criterion and an energy-based criterion. These lead to two different types of material parameters forming the basis for design of interfaces. A stress-based fracture criterion leads to the deflection-penetration criterion being expressed in terms of the relative strengths of the interface and second phase. An energy-based fracture criterion leads to the deflection-penetration criterion being expressed in terms of the relative toughnesses of the interface and second phase. At the present time, there is no crack deflection analysis that bridges these two historically distinct views of fracture. It is this gap in the understanding of the mechanics of interfaces that motivated the present study.

The cohesive-zone view provides a coherent analytical framework for fracture that naturally incorporates both strength and energy criteria. Cohesive-zone modeling has its origins in the early models of Dugdale [44] and Barenblatt [45] that considered the effects of finite stresses at a crack tip. A cohesive-zone model incorporates a region of material ahead of the crack (the "cohesive zone") having a characteristic traction-separation law that describes the fracture process. In a typical traction-separation law, the tractions across the crack plane increase with displacement up to a maximum cohesive strength, and then decay to zero at a critical opening displacement. When the critical displacement is reached, the material in the cohesive zone is assumed to have failed, and the crack advances. This approach to modeling fracture became particularly useful with the advent of sophisticated computational techniques, since it allowed crack propagation to be predicted for different geometries [46, 47, 48, 49, 50].

The fracture behavior in a single mode of deformation tends to be dominated by two characteristic quantities of the traction-separation law - a characteristic toughness (the area under the curve), Γ, and a characteristic strength (closely related to the cohesive strength for many traction-separation laws), $\hat{\sigma}$. Cohesive-zone models provide a particularly powerful approach for analyzing fracture since their predictions appear to be fairly insensitive to the details of the traction-separation law, being dependent only on these two characteristic parameters.[1]

The dependence of cohesive models on both strength and toughness parameters makes them a natural bridge between the two traditional views of fracture [53]. By varying the parameters of a cohesive model it is possible to move from a regime in which fracture is controlled only by the toughness, through a regime in which both toughness and strength control fracture, to a regime in which only strength dominates fracture. The relative importance of these two parameters is indicated by comparing the fracture-length scale, $E\Gamma/\hat{\sigma}^2$ (where E is the modulus of the material) to the appropriate characteristic length, L of the geometry [54]. When the fracture-length scale is relatively small, *i.e.*, the non-dimensional group $E\Gamma/\hat{\sigma}^2 L$ is very small, the toughness controls fracture; when the fracture-length scale is relatively large, the strength controls fracture. In the intermediate range, both parameters are important.

Consideration of the fracture-length scale immediately highlights an inherent problem with energy-based analyses of crack deflection at interfaces. These models invoke a pre-existing kink along the interface. This kink has to be very small in comparison to any other characteristic dimension of the problem, so that asymptotic solutions for the crack-tip stress field can be used. However, the length of the kink then becomes the characteristic dimension that the fracture-length scale must be compared to, in order to determine whether fracture is controlled by energy or stress. Therefore, the kink has to be short compared to any other dimensions of the problem, for crack-tip asymptotic solutions to be valid; but, simultaneously, the kink has to be long compared to the fracture length scale, so that an energy criterion for fracture is appropriate. If it is assumed that an interface can support singular stresses, the kink can be taken to the limit of zero length with no conceptual difficulty. *However, if an interface with a finite cohesive strength does not contain a physical kink of a finite length, both energy and stress are expected to play a role in initiating fracture along the interface.*

In this paper, a cohesive-zone model is used to analyze the problem of crack deflection at interfaces. Of major concern are (i) an elucidation of the roles of the interfacial strength, the interfacial toughness, the substrate strength and the substrate toughness on crack deflection, and (ii) an understanding of the conditions under

[1]The shape of the traction-separation curves can occasionally affect fracture. For example, there are laws in which the characteristic strength is not related to the cohesive strength [51, 52].

which any of these parameters might dominate design considerations. These issues are addressed by using a cohesive-zone analysis to look at the general problem of crack deflection at different fracture-length scales, in the absence of any pre-existing kinks. The results of the calculations are presented in non-dimensional terms for a wide range of parameter space, so that the effects of different strength and toughness values on the transition are fully explored. The roles of mixed-mode failure criteria and modulus mismatch across the interface are also explored. Finally, in the Appendix, cohesive-zone models are used to look at kinked cracks. The results of these calculations are used to make a connection with existing energy-based analyses of crack deflection, and to show that the numerical approach used in this paper can accurately capture the classical energy-based criteria for this phenomenon, provided the fracture-length scales are small enough, and that appropriate assumptions about the kinks are made.

2 Numerical Results

2.1 Cohesive-zone model

A cohesive-zone model was used to analyze crack deflection at interfaces. This problem requires a mixed-mode implementation of the model. Often, mixed-mode effects are modeled by combining normal and shear displacements into a single parameter that is used in a traction-separation law to indicate overall load-carrying ability [55]. However, an alternative approach is to use separate and independent laws for mode I and mode II, each being functions of only the normal and shear displacements, respectively. The ability to specify the mode-I and mode-II strength and toughness values independently appears to be necessary to capture some experimental results [56, 57, 58]. Since the traction-separation laws are prescribed independently, they need to be coupled through a mixed-mode failure criterion. Such a failure criterion relates the normal and shear displacements at which the load-bearing capability of the cohesive-zone elements fail. In this work, a linear failure criterion of the form

$$\mathcal{G}_I/\Gamma_I + \mathcal{G}_{II}/\Gamma_{II} = 1 \tag{2}$$

was used, where $\mathcal{G}_I$ is the mode-I energy-release rate, Γ_I is the mode-I toughness, $\mathcal{G}_{II}$ is the mode-II energy release rate, and Γ_{II} is the mode-II toughness. In this formulation, the toughness is defined as the total area under the traction-separation law, and the energy-release rate is defined as the area under the traction-separation law at any particular instant of interest [56]. While simple, this linear criterion allows for a fairly rich range of mixed-mode behavior to be mimicked, from what we will call a "Griffith criterion" for which there is a single value of the critical energy-release rate required for fracture (*i.e.*, $\Gamma_{II} = \Gamma_I$), to one in which fracture occurs only in response to mode-I loading ($\Gamma_{II} \gg \Gamma_I$). The use of Eqn. 2 in cohesive-zone analyses has been shown to do an excellent job of describing experimental results [56, 57, 58],

and it can mimic mixed-mode fracture criteria for linear-elastic fracture mechanics (LEFM), if the phase angle is defined as

$$\psi = \arctan\sqrt{\mathcal{G}_{II}/\mathcal{G}_I}, \tag{3}$$

where ψ has its usual definition under LEFM conditions of $\psi = \arctan(K_{II}/K_I)$, and K_{II} and K_I are the nominal mode-II and mode-I stress-intensity factors acting at a crack tip [59].

The general forms of the mode-I and mode-II traction-separation laws used in this study are shown in Fig. 3. The mode-I cohesive strength is $\hat{\sigma}$, the mode-II cohesive strength is $\hat{\tau}$, the mode-I toughness is Γ_I, and the mode-II toughness is Γ_{II}. Generalized forms for the traction-separation laws have been used, as the precise shape does not generally have a significant effect on fracture. The strength and toughness (area under the curve) are the two dominant parameters that control fracture, and cracks can propagate only if both the stress and energy criteria are met. As discussed above, the use of separate mode-I and mode-II laws allows for a general investigation of fracture, encompassing problems in which shear fracture has physical significance and problems in which pure shear only results in slip, not fracture.

The cohesive-zone modeling was implemented within the commercial finite-element package ABAQUS (version 6.3-1), as described by Yang [60]. Three- and four-node, linear, plane-strain elements were used for the continuum elements. The elements for the cohesive zone were defined using the ABAQUS UEL feature, the traction-separation laws of Fig. 3, and the failure criterion of Eqn. 2. These were implemented in a FORTRAN subroutine. An example of the code used is given in Ref. [61].

While several different geometries could have been used to study the problem of crack deflection, the work in this paper focuses on a laminated system subject to a uniform tensile displacement, as shown in Fig. 4. A layer of thickness h, with an elastic modulus of E_f and a Poisson's ratio of ν_f, is bonded to a substrate of thickness d. The layer of thickness h has a crack that extends from the free surface to the interface, and that is normal to the interface. The substrate has an elastic modulus of E_s and a Poisson's ratio of ν_s. For all the calculations reported in this paper, the substrate is ten times thicker than the cracked layer, so that $d = 10h$. Plane-strain conditions are assumed, so that the two Dundurs parameters can be defined as [62]

$$\alpha = \frac{\bar{E}_f - \bar{E}_s}{\bar{E}_f + \bar{E}_s}, \tag{4}$$

and

$$\beta = \frac{\bar{E}_f(1-2\nu_s)/(1-\nu_s) - \bar{E}_s(1-2\nu_f)/(1-\nu_f)}{2(\bar{E}_f + \bar{E}_s)}, \tag{5}$$

where, $\bar{E} = E/(1-\nu^2)$. If the substrate cracks, it will do so under pure mode-I conditions; therefore, only the mode-I fracture properties of the substrate are required. The mode-I substrate toughness is designated as Γ_s, and the mode-I strength is designated as $\hat{\sigma}_s$. The interface fails under mixed-mode conditions, and a mixed-mode analysis is required for crack propagation along the interface. The mode-I cohesive parameters of the interface are designated as Γ_{Ii} and $\hat{\sigma}_i$, while the mode-II cohesive parameters of the interface are designated as Γ_{IIi} and $\hat{\tau}_i$.

2.2 Effects of fracture length-scales on crack deflection

In this section, a general study of the effect of fracture parameters on crack deflection is presented. A macroscopic crack is assumed to impinge directly on an interface as shown in Fig. 4. There are no pre-existing kinks or flaws ahead of this main crack, and there is an axis of symmetry along the plane of the crack. Two rows of cohesive elements are placed at the tip of the crack; one row along the interface, and the other row in the substrate. A uniform tensile displacement is applied to the ends of the specimen. The required mesh density for the numerical calculations was determined by selecting several meshes, running the simulations, and analyzing the results to verify what mesh density gave consistent solutions that were within an acceptable range for the uncertainty of the results.

The transition between crack deflection and crack penetration for the geometry shown in Fig. 4 depends on the following material and geometrical parameters:

$$E_f, E_s, \nu_f, \nu_s, \Gamma_{Ii}, \Gamma_{IIi}, \Gamma_s, \hat{\sigma}_i, \hat{\tau}_i, \hat{\sigma}_s, h, d.$$

Using the Dundurs result for the effects of mismatched moduli across plane interfaces [62], these parameters can be re-expressed in the following non-dimensional groups for the plane-strain conditions considered in this paper:

$$\alpha, \beta, \Gamma_i/\bar{E}_f h, \bar{E}_f \Gamma_i/\hat{\sigma}_i^2 h, \hat{\sigma}_s/\hat{\sigma}_i, \Gamma_s/\Gamma_{Ii}, \Gamma_{IIi}/\Gamma_{Ii}, \hat{\tau}_i/\hat{\sigma}_i, d/h$$

The additional non-dimensional parameters δ_1/δ_c and δ_2/δ_c which describe the shape of the traction-separation laws (Fig. 3) were kept at constant values of 0.01 and 0.75 throughout the paper. These parameters do not play a significant role in the fracture process and transition in failure mechanism.

The quantity $\Gamma_i/\bar{E}h$ was fixed at 1.0×10^{-6} for all the results presented in this paper. This is a physically reasonable value for the parameter, and numerical studies indicated that even fairly significant changes around this level had a negligible influence on the failure transition. The initial studies were conducted with $\alpha = 0$, and $\beta = 0$ (so that $E_f = E_s = E$, and $\nu_f = \nu_s = \nu$), and with $\Gamma_{Ii} = \Gamma_{IIi} = \Gamma_i$ and $\hat{\tau}_i = \hat{\sigma}_i$. With these parameters fixed, a series of calculations was performed

holding the non-dimensional interface fracture-length scale at a constant value of $\bar{E}\Gamma_i/\hat{\sigma}_i^2 h = 0.01$. After running numerical calculations with a given set of $\hat{\sigma}_s/\hat{\sigma}_i$ and Γ_s/Γ_i, a note was made as to whether the crack first began to grow along the interface or through the substrate. In these calculations, the onset of crack growth along either plane was defined as occurring when the first element in a cohesive zone failed.[2]

A systematic exploration of how the failure mechanism depended on the magnitude of $\hat{\sigma}_s/\hat{\sigma}_i$ and Γ_s/Γ_i allowed a failure-mechanism map to be plotted, as shown in Fig. 5. In this figure, which has axes of $\hat{\sigma}_s/\hat{\sigma}_i$ and Γ_s/Γ_i, constant values of the non-dimensional substrate fracture-length scale follow a parabolic form. The error bars on this figure are associated with numerical considerations, and show the uncertainty with which the boundary of the transition could be determined. In this context, it should be noted that, occasionally, the demands of the geometry created numerical difficulties close to the transition. In the worst cases, the numerical simulation failed before the onset of crack growth. When this happened, the transition was quantified by examining the values of $\mathcal{G}_p/\Gamma_s$ and $\mathcal{G}_d/\Gamma_i$ at the point of the numerical instability, where $\mathcal{G}_p$ is the energy-release rate for penetration of the crack into the substrate and $\mathcal{G}_d$ is the energy-release rate for deflection of the crack along the interface. These ratios measure the extent of the appropriate traction-separation law that has been traversed, and indicate how close the elements of the cohesive zone are to failure.

As might be intuitively expected, the failure-mechanism map of Fig. 5 shows that crack deflection is promoted by high values of both $\hat{\sigma}_s/\hat{\sigma}_i$ and Γ_s/Γ_i. Conversely, crack penetration is promoted by low values of these two ratios. At larger values of the non-dimensional substrate fracture-length scale, the failure mechanism is controlled by the strength ratio; at smaller values, it becomes more sensitive to the toughness ratio. However, even in this latter range, there is no indication that only toughness controls the failure mechanism. Indeed, if there is a lower bound on the toughness ratio required to guarantee crack penetration, it is much lower than the range that could be explored by the present calculations. Conversely, there does appear to be a vertical asymptote representing a critical value of the strength ratio *below which crack penetration is guaranteed, irrespective of the toughness ratio.* This implies that crack penetration will always occur if the substrate strength is less than about three times greater than the interface strength, which is very consistent with the results of strength-based criteria [26, 28].

Non-dimensional fracture-length scales that are of the order of 0.01 for both the interface and substrate should be considered to represent linear-elastic conditions [53]. It is therefore of interest to note that a deflection criterion based solely on energy con-

[2]The issue of whether a crack might kink off an interface, after first deflecting along it, was not explored here. However, crack deflection off interfaces has been studied experimentally and modeled using a cohesive-zone approach in a paper by Li *et al.* [51].

siderations is not captured in this analysis.[3] Even in the linear-elastic regime, both the strength and toughness ratios determine the failure mechanism. However, as demonstrated in the Appendix, the deflection criterion of He and Hutchinson [37, 40] can be reproduced by the cohesive-zone model if pre-existing kinks are included in the analysis, as they are in the classical energy-based analyses. In the complete absence of a physical kink at the interface, a finite interface strength is always going to cause the interface fracture-length scale to violate the conditions for only an energy-criterion to be valid. Therefore, both strength and energy should be expected to play a role in initiating a crack along the interface from a crack that impinges the interface; and, hence, both strength and energy will determine the failure mechanism.

The approach used to produce Fig. 5 was extended to look at the effect of increasing the fracture-length scale of the interface, away from linear-elastic conditions. The calculations were repeated for additional values of $\bar{E}\Gamma_i/\hat{\sigma}_i^2 h = 0.1, 1.0$ and 10. The corresponding failure-mechanism maps are plotted in Fig. 6. On this figure, the boundaries (with appropriate error bars) between deflection and penetration are drawn for the different values of $\bar{E}\Gamma_i/\hat{\sigma}_i^2 h$. The basic form of the failure-mechanism map does not change as this quantity is varied, but the tendency for crack deflection appears to be reduced as the interface fracture-length scale is increased. The apparent vertical asymptote observed in Fig. 5 appears to be a general phenomenon, with the precise value of the critical strength ratio depending on the interfacial fracture-length scale. In addition, the fact that crack deflection can occur with relatively tough interfaces, provided the interfacial strength is low enough, also appears to be a general feature. Furthermore, the form of Fig. 6 suggests that there may be an asymptotic curve for very low values of $\bar{E}\Gamma_i/\hat{\sigma}_i^2 h$. This asymptotic behavior was explored by keeping $\bar{E}\Gamma_s/\sigma_s^2 h = \bar{E}\Gamma_i/\sigma_i^2 h$, and systematically decreasing them both. The results, plotted in Fig. 7, clearly show an asymptotic value of $\hat{\sigma}_s/\hat{\sigma}_i \approx 3.2$, below which crack penetration always occurs. It is interesting that this is very close to the strength-based, linear-elastic results of Gupta *et al.* [28], which predict a value of approximately 3.4 for the maximum ratio of the substrate to interface strength required for crack penetration in a homogeneous system.

[3] If one assumes self-similar traction-separation laws for the substrate and interface, so that $\hat{\sigma}_s/\hat{\sigma}_i = \Gamma_s/\Gamma_i$, Fig. 5 indicates that the transition in failure mechanism occurs when both the strength and toughness ratios are equal to about four. If one focuses only on the toughness ratio, this might appear to match the criterion of Refs. [38, 37], as noted in an earlier cohesive-zone analysis in which the strength and toughness ratios were related in this fashion [63]. However, this match should probably be considered to be coincidental, since Fig. 5 shows the failure mechanism actually depends on both the strength and toughness. Furthermore, there is probably no reason to expect such a relationship between the fracture parameters of the interface and substrate to be universally valid, especially when the interface consists of a bonding layer that is different from the substrate.

2.3 Effects of modulus mismatch on crack deflection

To explore the effects of modulus mismatch on crack deflection, the calculations were repeated for non-zero values of α, but leaving $\beta = 0$. Some failure-mechanism maps for $\alpha \neq 0$ are shown in Fig. 8. The general features of the transition curves do not appear to depend on the modulus mismatch. However, an interesting feature of the plots is that the tendency for penetration seems to be particularly pronounced when the cracked layer and substrate have comparable values of stiffness. Further investigations showed that crack deflection is very sensitive to mixed-mode effects at the interface, and that the particular behavior indicated in Fig. 8 can be attributed to the assumption of a Griffith failure criterion ($\Gamma_{IIi}/\Gamma_{Ii} = 1$).

As discussed earlier, the magnitude of the mode-II effects is quantified by the ratio of $\mathcal{G}_{II}/\mathcal{G}_I$ for the interface when the crack is just about to propagate. A detailed analysis of the present results showed that mode-II effects become dominant as α increases (as the cracked layer becomes stiffer). This observation is consistent with the results of He and Hutchinson [37, 40] that indicate the phase angle at the tip of an interface kink increases as the cracked layer becomes much stiffer than the substrate. In this regime, a Griffith criterion might be expected to give significantly different predictions from a mode-I dominated fracture criterion. Conversely, as the cracked layer becomes more compliant than the substrate, the interfacial fracture becomes increasingly dominated by mode-I deformation. In this regime, the distinction between a Griffith criterion and a mode-I dominated criterion becomes less critical. In this context, it is of interest to note that the deflection / penetration criterion of Gupta *et al.* [28] was based on a comparison of the normal stresses in the penetrating and deflecting directions with the normal interface and substrate strengths, without considering mode-II effects. This resulted in a conclusion that deflection should require decreasing interfacial strengths as the compliance of the substrate increases; it gets harder to deflect a crack if α increases (as defined in the present paper). The results of He and Hutchinson [37, 40] were presented in a fashion that was independent of failure criterion. However, by incorporating different mixed-mode fracture criteria into the results of those papers, it can be seen that a Griffith criterion results in crack penetration being most pronounced when the two layers have similar elastic constants, while a mode-I dominated criterion results in the same conclusion as Ref. [28].

These issues were examined within the present context by increasing the ratio of mode-II to mode-I interfacial toughness, from $\Gamma_{IIi}/\Gamma_{Ii} = 1$ to $\Gamma_{IIi}/\Gamma_{Ii} = 100$. As Eqn. 2 indicates, this increase in the ratio of Γ_{IIi}/Γ_{Ii} has the effect of making fracture along the interface become dominated by mode-I deformation only. Some results are shown in Fig. 9, in which the critical ratios of the substrate to interfacial strength required to guarantee crack penetration are plotted as functions of the modulus ratio. As can be seen from this plot, the critical stress ratio increases monotonically with α for a mode-

I fracture criterion ($\Gamma_{IIi}/\Gamma_{Ii} = 100$), but exhibits a maximum close to $\alpha = 0$ for the Griffith criterion ($\Gamma_{IIi}/\Gamma_{Ii} = 1$). The conclusions about how the modulus mismatch affects crack deflection are consistent with the earlier analyses, and further emphasize the importance of mixed-mode failure criteria on the deflection and penetration of cracks at interfaces.

3 Conclusions

Whether a crack that impinges on an interface between two materials will deflect along the interface, or penetrate through it, is an important aspect of the behavior of composites and multi-layered materials. While there are a number of analyses in the literature to describe this behavior, these are predicated on either an energy-based or a strength-based approach to fracture. In the present work, these distinct approaches have been combined through a cohesive-zone model of fracture, in which the toughness and the strength parameters of the interface and substrate (or fiber) all play a role. The analyses in this paper have been conducted for the particular geometry of a layered material, with a crack extending down from a free surface to the interface. However, while it is expected that the quantitative details of the results may depend on the precise geometry assumed for the problem, it is not expected that the important results will be qualitatively different. Therefore, the major conclusions presented in this paper as to how the strengths and toughnessses of an interface and second phase interact to determine whether crack deflection or penetration occurs, are expected to be valid for other geometries such as fiber-reinforced composites and polycrystalline materials. Of particular significance, is that, generally, both the strength and toughness parameters control the behavior in tandem.

Currently, it appears to be generally accepted that crack deflection requires the presence of interfaces that have a toughness less than one-quarter the toughness of the second phase (or substrate). This result derives from analyses invoking an energy-based fracture criterion in which the load required to propagate a *small pre-existing kink* along the interface is directly compared to the load required for the crack to penetrate past an interface *in which there is no kink*. In the Appendix, it is shown that a cohesive-zone analysis reproduces this result in the appropriate limit where the characteristic fracture length of both the interface and substrate are small in comparison to the length of the kink. However, if a crack impinges upon an interface that does not contain a pre-existing defect, then any real interface with a finite strength will have a fracture-length scale that is too large for energy-based analyses to be valid. It is this problem of crack deflection in the absence of pre-existing flaws that has been emphasized in this work.

The analysis has shown that crack deflection can be induced in systems with relatively tough but weak interfaces. In particular, deflection can occur even when the

interface is significantly tougher than the substrate, provided the strength of the interface is low enough. This would seem to be an important consideration in applications where a polymer or metal layer bonds two relatively strong brittle materials such as ceramics. It might perhaps be of particular importance in biological applications where bonding between brittle inorganic components of a material are provided by a protein layer.

The analysis has also indicated that there is a critical ratio for the substrate strength to the interface strength below which penetration will always occur. Below this critical ratio, the crack will not deflect along the interface, no matter how brittle the interface is nor how tough the substrate is. In particular, crack penetration appears to be guaranteed if the strength of the substrate is less than about three times the interface strength, with the precise value depending on the fracture-length scale and on the elastic mismatch in the system. The magnitude of this critical ratio is in excellent agreement with existing strength models for crack deflection.

It appears that the effects of mixed-mode fracture criteria are particularly important for determining the behavior of systems in which the cracked layer is much stiffer than the substrate. Under these conditions, mode-II effects contribute significantly to interfacial fracture, and the behavior of the system becomes very sensitive to the mixed-mode failure criterion. If delamination is controlled by a Griffith fracture criterion, with the response of the interface being identical to both mode-I and mode-II deformation, then the tendency for crack deflection is enhanced by having a modulus mismatch between the substrate and cracked layer. Crack penetration is most likely when the modulus of the substrate and cracked layer are similar; increasing the stiffness of either layer increases the tendency for deflection. If, however, delamination is controlled by a mode-I dominated failure criterion, then the tendency for deflection is enhanced only by increasing the modulus of the substrate. An increase in the stiffness of the cracked layer increases the tendency for penetration.

Finally, it is noted that three related issues in crack deflection have not been addressed in the present study; these are left as possible areas of future studies. The first issue is how a crack interacts with a pre-existing flaw on the interface. Such a study would require suitably oriented cohesive elements at the tip of the interfacial flaw to capture the possibility of substrate failure initiating from the tip of the kink. The second issue is the extent to which such a pre-existing flaw might be generated by the stress field of an approaching crack. The third issue is whether a crack can deflect out of an interface after delamination has proceeded some way along the interface. Such a study would require suitably oriented cohesive elements in the substrate distributed along the interface. Some preliminary insights into this last problem have already been provided by Li *et al.* [51], which demonstrates that the strength parameters (as well as the toughness parameters) do play an important role in determining

whether a crack kinks off a relatively brittle adhesive interface into a much tougher composite. These results reinforce the essential message of the work presented in this present paper that a full understanding of crack deflection at interfaces requires both the toughness and strength parameters of the interface and surrounding material to be considered.

Acknowledgments

The authors would like to thank Dr. S. Li for useful discussions and comments during the course of this project.

A Appendix: Effect of kinks on crack deflection

The work of He *et al.* [37, 40] provides a very complete energy-based analysis of the conditions under which a crack will deflect when it impinges upon an interface. In this Appendix, the cohesive-zone approach is used to study crack deflection under conditions for which this type of analysis is valid. As in the original analysis, the calculations were conducted as a comparison between the two distinct geometries illustrated in Fig. 10: one with a small double kink extending along the interface ahead of the main crack, each of length k; and the other with a small kink, also of length k, extending across the interface into the substrate. In both geometries, a macroscopic crack of length h extends from the free surface to the interface, and a set of cohesive-zone elements extends ahead of the kink. It should be noted that the fact of two separate geometries being used in the analysis provides a subtle variation from the fundamental problem of how a single crack meeting an interface will propagate.

The calculations were done for the special conditions of $E_f = E_s = E$, $\nu_f = \nu_s = \nu$, $\hat{\tau}_i = \hat{\sigma}_i = \hat{\sigma}_s$, and $\Gamma_{Ii} = \Gamma_{IIi} = \Gamma_i$. This results in the following dimensionless groups describing the two problems:

$$\begin{aligned} &\Gamma_i/\bar{E}k, \bar{E}\Gamma_i/\hat{\sigma}_i^2 k, k/h, d/h && \text{(deflection)} \\ &\Gamma_s/\bar{E}k, \bar{E}\Gamma_s/\hat{\sigma}_s^2 k, k/h.d/h && \text{(penetration).} \end{aligned}$$

In this analysis, d/h was kept constant at $d/h = 10$. Reproducing the energy-based analysis [37, 40] placed several constraints on the analysis. First, the kink had to be small in comparison to h, so that boundary effects would not influence the stresses near the kink. Second, the fracture properties had to be such that linear-elastic fracture mechanics (LEFM) conditions were satisfied not only at the macroscopic scale, but also at the scale of the kink length, *i.e.*, both $\bar{E}\Gamma_i/\hat{\sigma}_i^2 k$ and $\bar{E}\Gamma_s/\hat{\sigma}_s^2 k$ had to be very small. In this analysis, LEFM conditions were maintained by setting $\bar{E}\Gamma_i/\hat{\sigma}_i^2 k = 0.01$; while $\bar{E}\Gamma_s/\hat{\sigma}_s^2 k$ was allowed to vary, it did not exceed limits for which LEFM conditions are expected to apply. Third, the mesh size had to be very small with respect to the kink length in order to generate accurate results. This last constraint, coupled with the fact that the kinks themselves had to be very small with respect to the overall geometry, resulted in an extremely fine mesh density being required to perform the calculations. The appropriate mesh density for the numerical calculations was determined by selecting several meshes, running the simulations, and analyzing the results to verify that the solutions were consistent within an acceptable range of uncertainty for the results. At the most extreme conditions studied, the kink was five orders of magnitude less than the thickness of the layer, h, and the mesh size was yet another five orders of magnitude smaller than this.

The calculations were performed by doing a numerical analysis on the geometries shown in Fig. 10, keeping $\Gamma_i/\bar{E}k$ at a constant value of 10^{-6}. First, the calcula-

tion was done for the geometry with a double kink extending along the interface, to determine the load at which the crack propagated for a given kink length. Then, a second set of calculations was done using this load for the geometry with a single kink of the same length extending across the interface and into the substrate. The applied load was kept constant, while the value of the substrate toughness that would just permit the crack to propagate was determined. The ratio between this value of toughness and the corresponding toughness of the interface was then taken to be the critical value for the transition between crack deflection and crack penetration.

The applied stress required to propagate an interfacial crack, σ_d, is plotted as a function of the kink length in Fig. 11. This plot follows the form predicted using linear-elastic fracture mechanics for the identical geometry in Thouless *et al.* [38], with the strength rising with kink length over the range of kink lengths shown. (Eventually, the strength is expected to reach the steady-state delamination value of $1.17\sqrt{\bar{E}\Gamma_i/h}$, for this geometry where the substrate is ten times the layer thickness [59].) The asymptotic limit at very small kink lengths can be determined from the results of He *et al.* [37, 40]. For a homogeneous system, the energy-release rate acting to propagate a very short kink along the interface is related to the applied mode-I stress-intensity factor, K_1 by [37, 40]

$$\mathcal{G}_d = 0.2608 K_1^2/\bar{E}. \tag{6}$$

If the substrate is ten times thicker than the cracked film, then K_1 is [64]

$$K_1 = 1.197\sigma_o\sqrt{\pi h}, \tag{7}$$

where σ_o is the remote applied stress. Hence, the remote applied stress required to propagate a very short kink along the interface is given by

$$\sigma_d = 0.923\sqrt{\bar{E}\Gamma_i/h}. \tag{8}$$

It can be seen from Fig. 11 that this asymptotic limit is in excellent agreement with the present results, which were obtained by keeping the ratio of the interface fracture-length scale to the kink length fixed at a very small value.

The corresponding phase angles at the onset of fracture for the interfacial kink were determined using Eqn. 3, with the values of $\mathcal{G}_{II}$ and $\mathcal{G}_I$ taken as the area of the interfacial traction-separation curves traced out up to the point of fracture. These phase angles are plotted in Fig. 12. As expected, the phase angle rises from the asymptotic value of 38.9^o given in Ref. [40] for a double kink in a homogeneous system, towards the value of 54.6^o that would be expected for the steady-state delamination crack appropriate for this geometry [59].

The critical ratio of the substrate toughness to the interface toughness for the transition between crack deflection and crack penetration (for equal sized kinks and

the same applied loads) is plotted in Fig. 13, as a function of kink length. Equation 7 can be combined with the results of Ref. [40] to write down an expression for this ratio as

$$\Gamma_s/\Gamma_i = 3.83 + 5.77(k/h)^{1/2} + 2.18(k/h). \tag{9}$$

As can be seen from Fig. 13, this expression is in excellent agreement with the numerical results presented here. Therefore, it has been demonstrated that the cohesive-zone model used in this study does an excellent job of computing the linear-elastic behavior of cracks at interfaces with equal-length kinks extending either along the interface or into the substrate. It should be emphasized that as k/h was reduced in these numerical calculations, it was done so keeping $\bar{E}\Gamma_i/\hat{\sigma}_i^2 k$ at a constant value of 0.01. If the calculations had been performed in such a fashion that the kink length had decreased significantly compared to the interface fracture-length scale, the results would have deviated from Eqn. 9, as k/h tended to zero.

It should be noted that performing this comparison between two different kinked-crack geometries is not necessarily equivalent to solving the particular problem of interest in this study, which is to determine the behavior of a crack meeting an interface. For example, the comparison between two distinct geometries cannot include possible effects of the interfacial kinks shielding the crack from penetrating the substrate. This lack of shielding is probably responsible for the counter-intuitive conclusion of Fig. 13 that longer pre-existing kinks on an interface make penetration more, rather than less, likely. In addition, if one is interested in the fundamental problem of a crack impinging an interface with no pre-existing defects, one cannot take an energy-based argument to its logical extreme of zero kink length because, in that limit, the fracture-length scale for any practical material will always be large compared to the kink, and the strength parameter will play an important role in the behavior. It is this last issue that was addressed in the bulk of this paper.

References

[1] G H Campbell, M Ruhle, B J Dalgleish, and A G Evans. Whisker toughening: A comparison between aluminum oxide and silicon nitride toughnened with silicon carbide. *Journal of the American Ceramic Society*, 73(3):521–30, 1990.

[2] A G Evans and D B Marshall. The mechanical behavior of ceramic matrix composites. *Acta Metallurgica*, 37:2567–2583, 1989.

[3] J Aveston, G A Cooper, and A Kelly. The properties of fiber composites. In *Conference Proceedings, National Physical Laboratory (IPC Science and Technology Press Ltd Paper 1*, page 1, 1971.

[4] J Aveston and A Kelly. Theory of multiple fracture of fibrous composites. *Journal of Materials Science*, 8:352–362, 1973.

[5] A G Evans, M Y He, and J W Hutchinson. Interface debonding and fiber cracking in brittle matrix composites. *Journal of the American Ceramic Society*, 72:2300–2303, 1989.

[6] M Ruhle, B J Dalgeish, and A G Evans. On the toughening of ceramics by whiskers. *Scripta Metallurgica*, 21(5):681–686, 1987.

[7] P F Becher and G C Wei. Toughening behavior in sic-whisker-reinforced alumina. *Journal of the American Ceramic Society*, 76(12):C267–C269, 1984.

[8] A Khan, H M Chan, M P Harmer, and R F Cook. Toughening of an alumina-mullite composite by unbroken bridging elements. *Journal of the American Ceramic Society*, 83(4):833–840, 2000.

[9] R F Cook. Segregation effects in the fracture of brittle materials. *Acta Metallurgica*, 38(6):1083–1100, 1990.

[10] K T Faber and A G Evans. Crack deflection processes - I. Theory. *Acta Metallurgica*, 31(4):565–576, 1983.

[11] K T Faber and A G Evans. Crack deflection processes - II. Experiment. *Acta Metallurgica*, 31(4):577–584, 1983.

[12] D Kovar, B H King, R W Trice, and J W Halloran. Fibrous monolithic ceramics. *Journal of the American Ceramic Society*, 80(10):2471–2487, 1997.

[13] D Kovar, M D Thouless, and J W Halloran. Crack deflection and propagation in layered silicon nitride and boron nitride ceramics. *Journal of the American Ceramic Society*, 81:1004–1012, 1998.

[14] W J Clegg. Fabrication and failure of laminar ceramic composites. *Acta Metallurgica et Materialia*, 40(11):3085–3093, 1992.

[15] H M Chan. Layered ceramics: Processing and mechanical behavior. *Annual Review of Materials Science*, 27:249–282, 1997.

[16] A M Korsunsky. Debounding of a weak interface in front of a through-thickness crack. *International Journal of Fracture*, 109(4):L35–L40, 2001.

[17] Z Xia, L Riester, W A Curtin, H Li, B W Sheldon, J Liang, B Chang, and J M Xu. Direct observation of toughening mechanisms in carbon nanotube ceramic matrix composites. *Acta Materialia*, 52(4):931–944, 2004.

[18] H Luo, D Goberman, L Shaw, and M Gell. Indentation fracture behavior of plasma-sprayed nanostructured Al_2O_3 - 13 wt% TiO_2 coatings. *Materials Science and Engineering A - Structural Materials Properties Microstructure and Processing*, 346(1-2):237–245, 2003.

[19] V C Nardone and K M Prewo. Tensile performance of carbon-fibre-reinforced glass. *Journal of Materials Science*, 23(1):168, 1988.

[20] C A Folsom, F W Zok, F F Lange, and D B Marshall. The mechanical behavior of a laminar ceramic/fiber-reinforced epoxy composite. *Journal of the American Ceramic Society*, 75(9):1223–28, 1992.

[21] M Y He, D J Heredia, D J Wissuchek, M C Shaw, and A G Evans. The mechanics of crack growth in layered materials. *Acta Metallurgica et Materiallia*, 41(4):1223–28, 1993.

[22] W-C Tu, F F Lange, and A G Evans. Concept for a damage-tolerant ceramic composite with strong interfaces. *Journal of the American Ceramic Society*, 79(2):417–24, 1996.

[23] M F Ashby and D R H Jones. *Engineering Materials 2; An Introduction to Microstructures, Processing, and Design.* Butterworth-Heinemann, Woburn, MA, 1998.

[24] S A Wainwright, W D Biggs, J D Currey, and J M Gosline. *Mechanical Design in Organisms.* Princeton University Press, Princeton NJ, 1982.

[25] H Kessler, E Chateau, R Ballarini, A H Heuer, and S M Spearing. Fracture mechanisms of the strombus gigas conch shell: Implications for the design of brittle laminates. *Journal of Materials Science*, 31(24):6583–6594, 1996.

[26] J Cook and J E Gordon. A mechanism for the control of crack propagation in all-brittle systems. *Proceedings of the Royal Society of London, Series A*, 282(139):508–520, 1964.

[27] C E Inglis. Stresses in a plate due to the presence of cracks and sharp corners. In *Proceedings of the Institute of Naval Architects*, volume 55, pages 219–230, 1913.

[28] V Gupta, A S Argon, and Z Suo. Crack deflection at an interface between two orthotropic media. *Journal of Applied Mechanics*, 59:S79–S87, 1992.

[29] A K Zak and M L Williams. Crack point singularities at a bi-material interface. *Journal of Applied Mechanics*, 30:142–143, 1963.

[30] M L Williams. On the stress distribution at the base of a stationary crack. *Journal of Applied Mechanics*, 24:109–114, 1957.

[31] D O Swenson and C A Rau. The stress distribution around a crack perpendicular to an interface between materials. *International Journal of Fracture Mechanics*, 6:357–360, 1970.

[32] J R Rice. Elastic fracture-mechanics concepts for interfacial cracks. *Journal of Applied Mechanics - Transactions of the ASME*, 55(1):98–103, 1988.

[33] A A Griffith. The phenomenon of rupture and flow in solids. *Philosophical Transactions of the Royal Society of London*, A221:163–198, 1920.

[34] G R Irwin. Analysis of stresses and strains near the end of a crack traversing a plate. *Journal of Applied Mechanics*, 24:364–364, 1957.

[35] J A Kies and H L Smith. *Toughness Testing of Hot-Stretched Acrylics*. Aircraft Industries Association and Air Development Command, Dayton OH, 1955.

[36] E Orowan. Fracture and strength of solids. *Reports on Progress in Physics*, 12:185–232, 1949.

[37] M Y He and J W Hutchinson. Crack deflection at an interface between dissimilar elastic materials. *International Journal of Solids and Structures*, 25(9):1053–1067, 1989.

[38] M D Thouless, H C Cao, and P A Mataga. Delamination from surface cracks in composite materials. *Journal of Materials Science*, 24:1406–1412, 1989.

[39] D Martinez and V. Gupta. Energy criterion for crack deflection at an interface between two orthotropic media. II. Results and experimental verification. *Journal of the Mechanics and Physics of Solids*, 42:1247—1271, 1993.

[40] M Y He, A G Evans, and J W Hutchinson. Crack deflection at an interface between dissimilar elastic materials: Role of residual stresses. *International Journal of Solids and Structures*, 31(24):3443–3455, 1994.

[41] M C Lu and F Erdogan. Stress intensity factors in two bonded elastic layers containing cracks perpendicular to and on the interface - I. Analysis. *Engineering Fracture Mechanics*, 18:491–506, 1983.

[42] D L Tullock, I E Reimanis, A L Graham, and J J Petrovic. Deflection and penetration of cracks between 2 dissimilar materials. *Acta Metallurgica et Materialia*, 42(9):3245–3252, 1994.

[43] B Cotterell and J R Rice. Slightly curved or kinked cracks. *International Journal of Fracture*, 16(2):155–169, 1980.

[44] D S Dugdale. Yielding of sheets containing slits. *Journal of the Mechanics and Physics of Solids*, 8:100–104, 1960.

[45] G I Barenblatt. The mathematical theory of equilirium cracks in brittle fracture. *Advances in Applied Mechanics*, 7:55–129, 1962.

[46] A Hillerborg, M Modeer, and P E Peterson. Analysis of crack formation and crack growth in concrete by means of fracture mechanics and finite elements. *Cement and Concrete Research*, 6:773–782, 1976.

[47] A Needleman. A continuum model for void nucleation by inclusion debonding. *Journal of Applied Mechanics*, 54:525–553, 1987.

[48] A Needleman. An analysis of decohesion along an imperfect interface. *International Journal of Fracture*, 42:21–40, 1990.

[49] V Tvergaard and J W Hutchinson. The relation between crack growth resistance and fracture process parameters in elastic plastic solids. *Journal of the Mechanics and Physics of Solids*, 40:1377–1392, 1992.

[50] T Ungsuwarungsri and W G Knauss. Role of damage-softened material behavior in the fracture of composites and adhesives. *International Journal of Fracture*, 35:221–241, 1987.

[51] S Li, M D Thouless, A M Waas, J A Schroeder, and P D Zavattieri. Use of mode-I cohesive-zone models to describe the fracture of an adhesively-bonded polymer-matrix composite. *Journal of Composites Science and Technology*, 65:281–293, 2005.

[52] S Li, M D Thouless, A M Waas, J A Schroeder, and P D Zavattieri. Use of a cohesive-zone model to analyze the fracture of a fiber-reinforced polymer-matrix composite. *Journal of Composites Science and Technology*, 65:537–549, 2005.

[53] J P Parmigiani and M D Thouless. Effects of the cohesive strength of interfaces on delamination phenomena. Manuscript in preparation.

[54] Z Suo, S Ho, and X Gong. Notch ductile-to-brittle transition due to localized inelastic band. *Journal of Engineering Materials and Technology*, 115:319–326, 1993.

[55] V Tvergaard and J W Hutchinson. The influence of plasticity on mixed mode interface toughness. *Journal of the Mechanics and Physics of Solids*, 41:1119–1135, 1993.

[56] Q D Yang and M D Thouless. Mixed-mode fracture analyses of plastically-deforming adhesive joints. *International Journal of Fracture*, 110:175–187, 2001.

[57] M S Kafkalidis and M D Thouless. The effects of geometry and material properties on the fracture of single lap-shear joints. *International Journal of Solids and Structures*, 39:4367–4383, 2002.

[58] S Li, M D Thouless, A M Waas, J A Schroeder, and P D Zavattieri. Mixed-mode cohesive-zone models for fracture of an adhesively-bonded polymer-matrix composite. *Journal of Engineering Fracture Mechanics*, in press.

[59] J W Hutchinson and Z Suo. Mixed mode cracking in layered materials. *Advances in Applied Mechanics*, 29:63–191, 1992.

[60] Q D Yang. *Fracture Analyses of Plastically-Deforming Adhesive Joints*. PhD thesis, University of Michigan, Ann Arbor, MI, 2000.

[61] J P Parmigiani. *Delamination and Deflection at Interfaces*. PhD thesis, University of Michigan, Ann Arbor, MI, 2005.

[62] J Dundurs. Edge-bonded dissimilar orthogonal elastic wedges. *Journal of Applied Mechanics*, 36:650–652, 1969.

[63] T Siegmund, N A Fleck, and A Needleman. Dynamic crack growth across an interface. *International Journal of Fracture*, 85:381–402, 1997.

[64] H Tada, P C Paris, and G R Irwin. *The Stress Analysis of Cracks Handbook, 2nd ed.* Paris Productions, Inc., St. Louis, MO, 1985.

Figure 1: Manifestations of crack deflection in composites and multi-layered materials. **(a)** Crack bridging in a fiber-reinforced composite. **(b)** Crack deflection in a whisker- or particle-reinforced composite. **(c)** Delamination in a laminated composite. **(d)** Delamination in a multi-layered film on a substrate.

Figure 2: Details of the crack deflection problem modeled by He and Hutchinson [37]. The macroscopic view is shown in **(a)**. A comparison is made between the conditions for **(b)** a small kink to extend across the interface, and **(c)** a small kink to extend along the interface.

Figure 3: Schematic illustration of the **(a)** mode-I, and **(b)** mode-II traction-separation laws used for the cohesive-zone model in this paper. Throughout this paper the values of δ_1/δ_c and δ_2/δ_c were kept at fixed values of 0.01 and 0.75 respectively.

Figure 4: The laminated geometry used to study crack deflection in this paper. A layer of thickness h and with an elastic modulus of E_f and a Poisson's ratio of ν_f is bonded to a substrate of thickness d, where $d = 10h$. The substrate has an elastic modulus of E_s and a Poisson's ratio of ν_s. There is a crack that extends from the top surface to the interface, and is normal to the interface. Sets of cohesive elements exist ahead of the crack in the substrate and along the interface. There is a plane of symmetry along the crack, and the system is loaded by a uniform displacement applied to the ends of the specimen.

Figure 5: The results of a set of calculations for $\bar{E}\Gamma_i/\hat{\sigma}_i^2 h = 0.01, \alpha = \beta = 0, \Gamma_i/\bar{E}h = 1.0 \times 10^{-6}, \Gamma_{Ii} = \Gamma_{IIi} = \Gamma_i, \hat{\sigma}_i = \hat{\tau}_i$, and $d/h = 10$. The plot shows the regimes in which crack penetration or crack deflection will occur in Γ_s/Γ_i and $\hat{\sigma}_s/\hat{\sigma}_i$ space. The error bars indicate the range of uncertainty of the transition.

Figure 6: The results of a set of calculations for $\bar{E}\Gamma_i/\hat{\sigma}_i^2 h = 0.01, 0.1, 1.0$ and 10.0. The values of the other non-dimensional groups for this plot are $\alpha = \beta = 0, \Gamma_i/\bar{E}h = 1.0 \times 10^{-6}, \Gamma_{Ii} = \Gamma_{IIi} = \Gamma_i, \hat{\sigma}_i = \hat{\tau}_i$, and $d/h = 10$. The plot shows the regimes in which crack penetration or crack deflection will occur in Γ_s/Γ_i and $\hat{\sigma}_s/\hat{\sigma}_i$ space. The error bars indicate the range of uncertainty of the transition.

Figure 7: A plot showing how the strength ratio and the toughness ratio for the transition between crack deflection and penetration vary with the normalized interface fracture-length scale. For this plot, the non-dimensional groups have values of $\bar{E}\Gamma_s/\hat{\sigma}_s^2 h = \bar{E}\Gamma_i/\hat{\sigma}_i^2 h, \alpha = \beta = 0, \Gamma_i/\bar{E}h = 1.0 \times 10^{-6}, \Gamma_{Ii} = \Gamma_{IIi} = \Gamma_i, \hat{\sigma}_i = \hat{\tau}_i$, and $d/h = 10$.

Figure 8: A failure mechanism map showing the effects of modulus mismatch. These calculations were done for $\bar{E}_f\Gamma_i/\hat{\sigma}_i^2 h = 0.01, \beta = 0, \Gamma_i/\bar{E}_f h = 1.0 \times 10^{-6}, \Gamma_{Ii} = \Gamma_{IIi} = \Gamma_i, \hat{\sigma}_i = \hat{\tau}_i$, and $d/h = 10$.

Figure 9: A plot showing the asymptotic strength ratio for the transition between crack deflection and crack penetration as a function of α for two different ratios of the mode-I and mode-II interfacial toughness, $\Gamma_{IIi}/\Gamma_{Ii} = 1$ and $\Gamma_{IIi}/\Gamma_{Ii} = 100$. These calculations were done for $\bar{E}_f\Gamma_i/\hat{\sigma}_i^2 h = 0.01, \beta = 0, \Gamma_i/\bar{E}_f h = 1.0 \times 10^{-6}, \hat{\sigma}_i = \hat{\tau}_i$, and $d/h = 10$.

Figure 10: Details of the two geometries used to study the effect of pre-existing kinks on crack deflection. **(a)** A cohesive zone extends ahead of a kink in the substrate. **(b)** A cohesive zone extends ahead of a kink along the interface.

Figure 11: The applied stress, σ_d, required to propagate a kink along the interface (normalized by $\sqrt{\bar{E}\Gamma_i/h}$), plotted as a function of kink length (normalized by h). In this plot the following non-dimensional groups were kept constant: $\bar{E}\Gamma_i/\hat{\sigma}_i^2 k = 0.01$, $\Gamma_i/\bar{E}k = 10^{-6}$, and $d/h = 10$.

Figure 12: The phase angles for an interfacial crack at the onset of fracture, as defined by Eqn. 3, plotted as a function of normalized kink length. In this plot the following non-dimensional groups were kept constant: $\bar{E}\Gamma_i/\hat{\sigma}_i^2 k = 0.01$, $\Gamma_i/\bar{E}k = 10^{-6}$, and $d/h = 10$.

Figure 13: The critical ratio of the substrate to interfacial toughness required to ensure that the load to propagate a kink along the interface is lower than the load to propagate a kink through the substrate. In this plot the following non-dimensional groups were kept constant: $\bar{E}\Gamma_i/\hat{\sigma}_i^2 k = 0.01$, $\Gamma_i/\bar{E}k = 10^{-6}$, and $d/h = 10$.

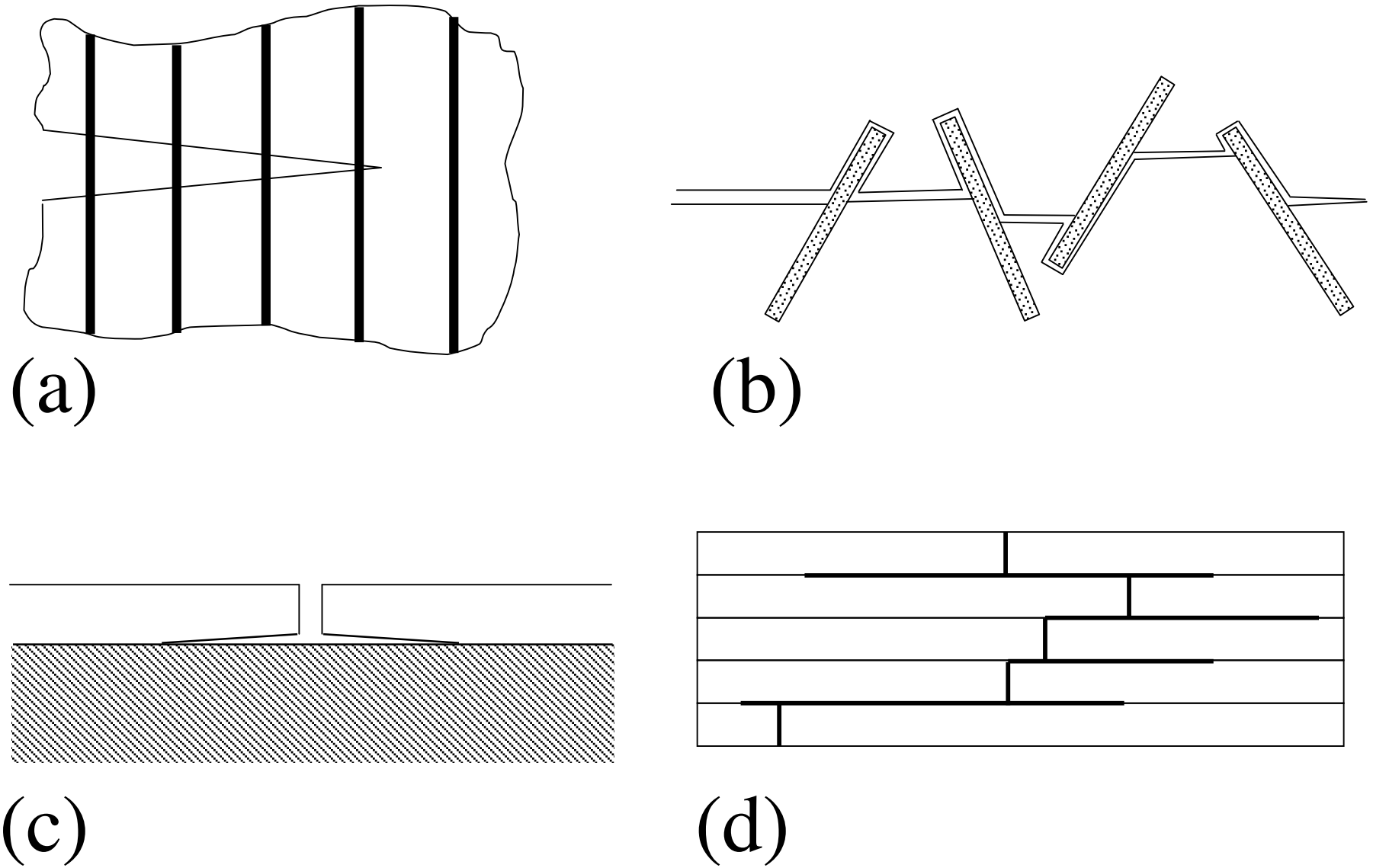

Figure 1

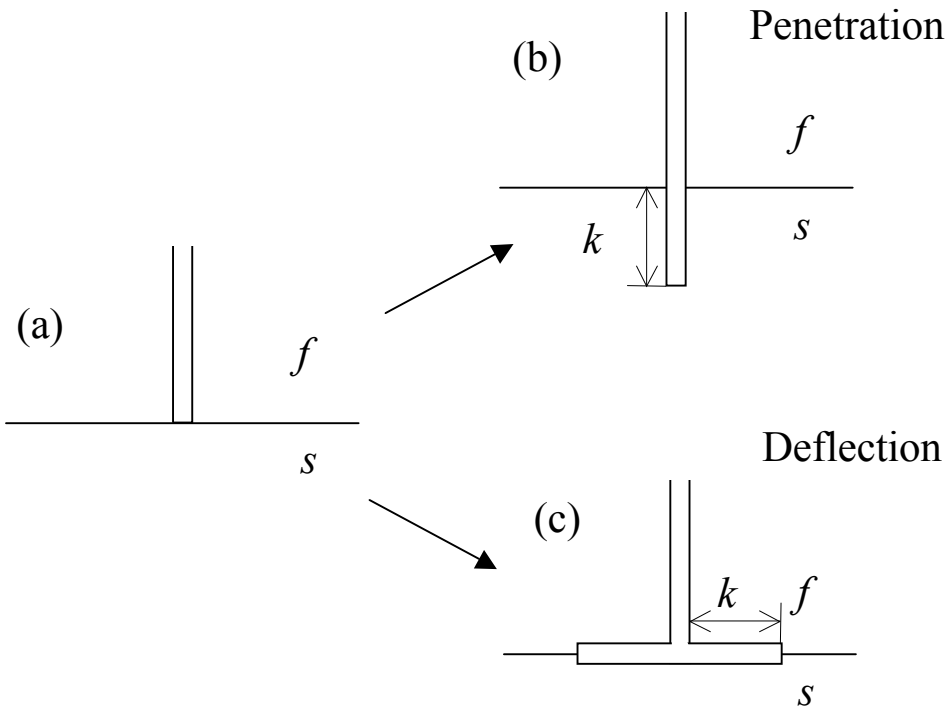

Figure 2

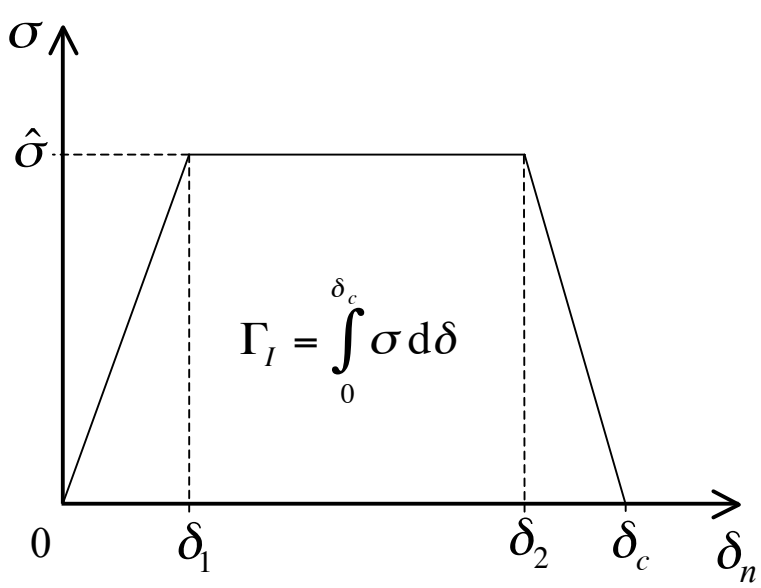

Mode I

(a)

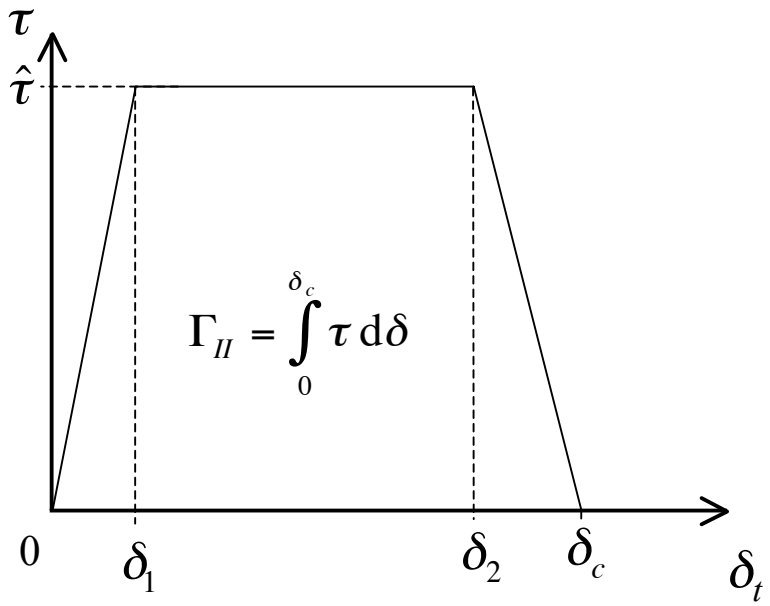

Mode II

(b)

Figure 3

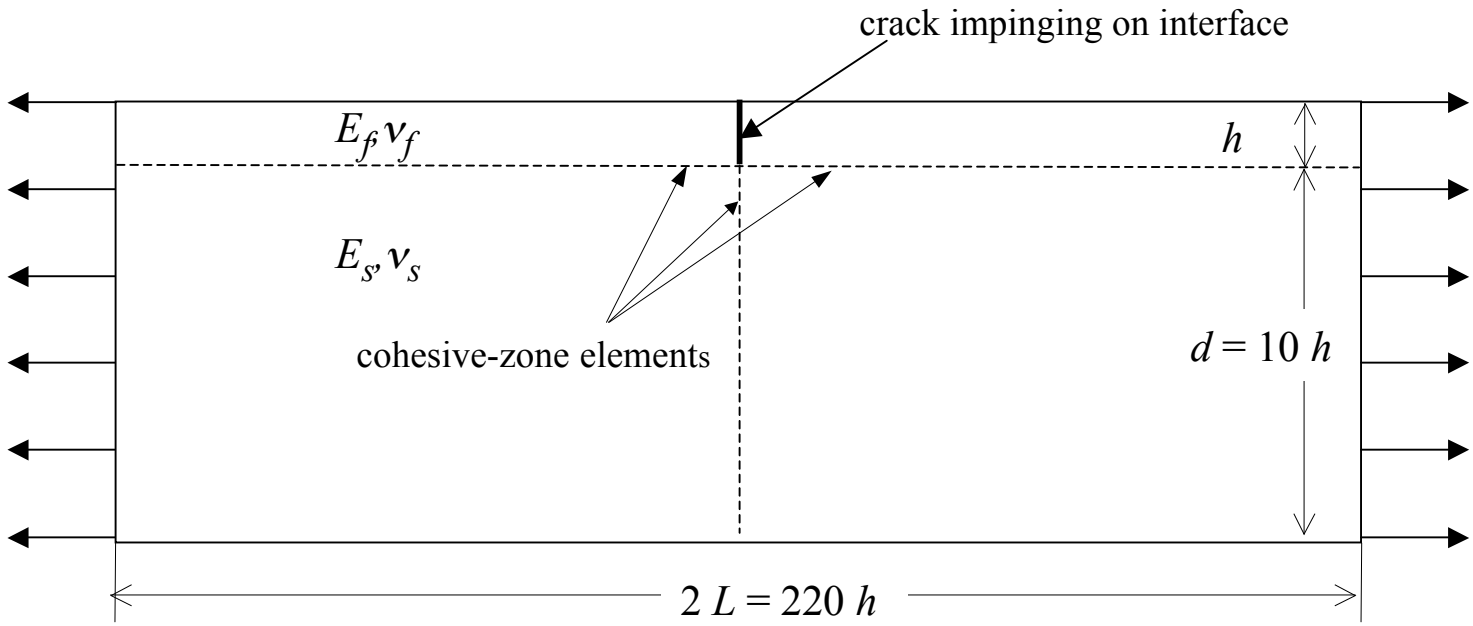
crack impinging on interface
E_f, ν_f
h
E_s, ν_s
cohesive-zone elements
$d = 10\ h$
$2\ L = 220\ h$

Figure 4

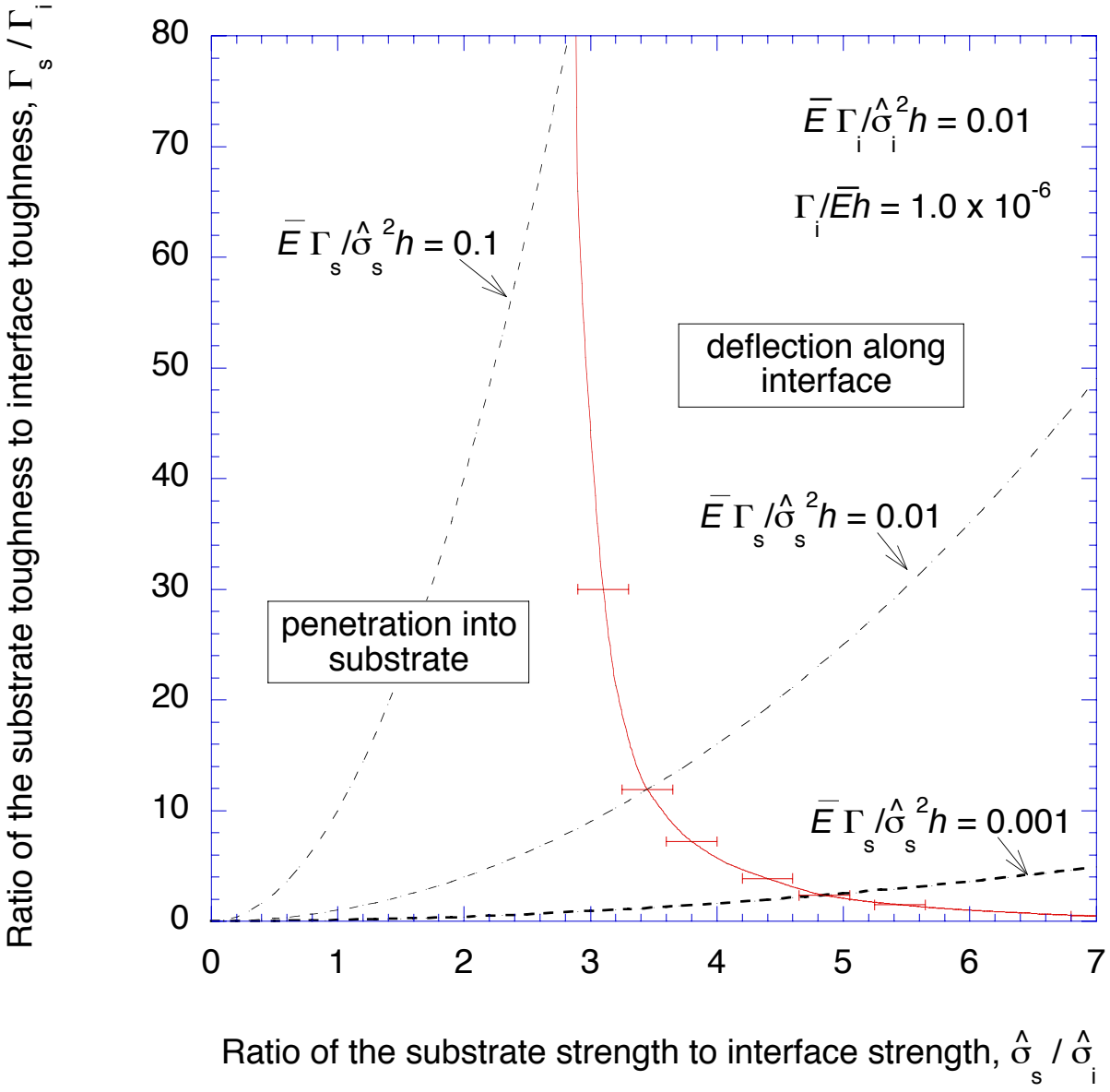
Ratio of the substrate toughness to interface toughness, Γ_s / Γ_i
80
70
60
50
40
30
20
10
0
0
1
2
3
4
5
6
7
$\bar{E}\,\Gamma_i/\hat{\sigma}_i^2 h = 0.01$
$\Gamma_i/\bar{E}h = 1.0 \times 10^{-6}$
$\bar{E}\,\Gamma_s/\hat{\sigma}_s^2 h = 0.1$
deflection along interface
$\bar{E}\,\Gamma_s/\hat{\sigma}_s^2 h = 0.01$
penetration into substrate
$\bar{E}\,\Gamma_s/\hat{\sigma}_s^2 h = 0.001$
Ratio of the substrate strength to interface strength, $\hat{\sigma}_s / \hat{\sigma}_i$

Figure 5

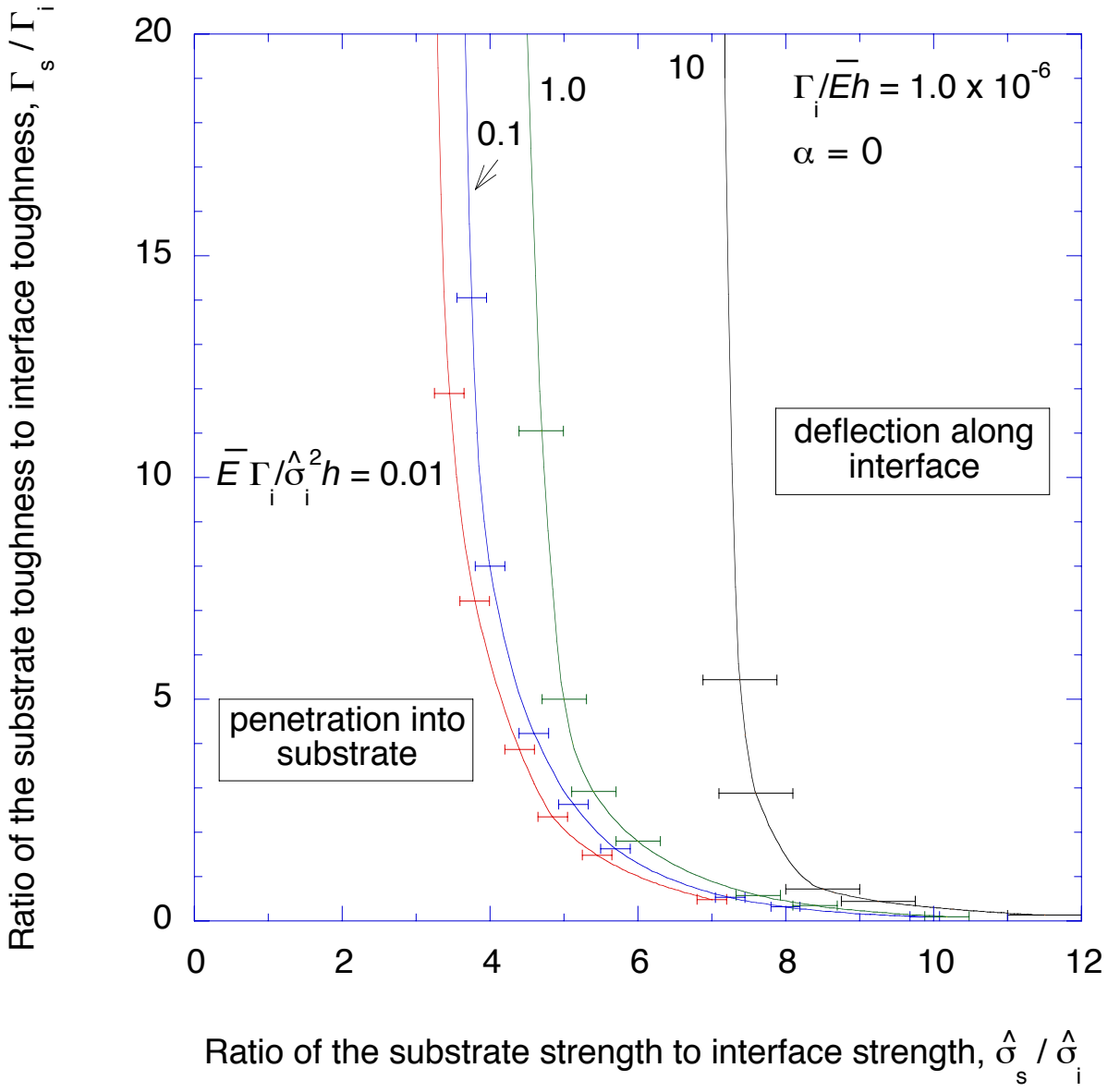
Ratio of the substrate toughness to interface toughness, Γ_s / Γ_i
Ratio of the substrate strength to interface strength, $\hat{\sigma}_s / \hat{\sigma}_i$
$\bar{E}\Gamma_i/\hat{\sigma}_i^2 h = 0.01$
$\Gamma_i/\bar{E}h = 1.0 \times 10^{-6}$
$\alpha = 0$
0.1
1.0
10
deflection along interface
penetration into substrate
0
5
10
15
20
0
2
4
6
8
10
12

Figure 6

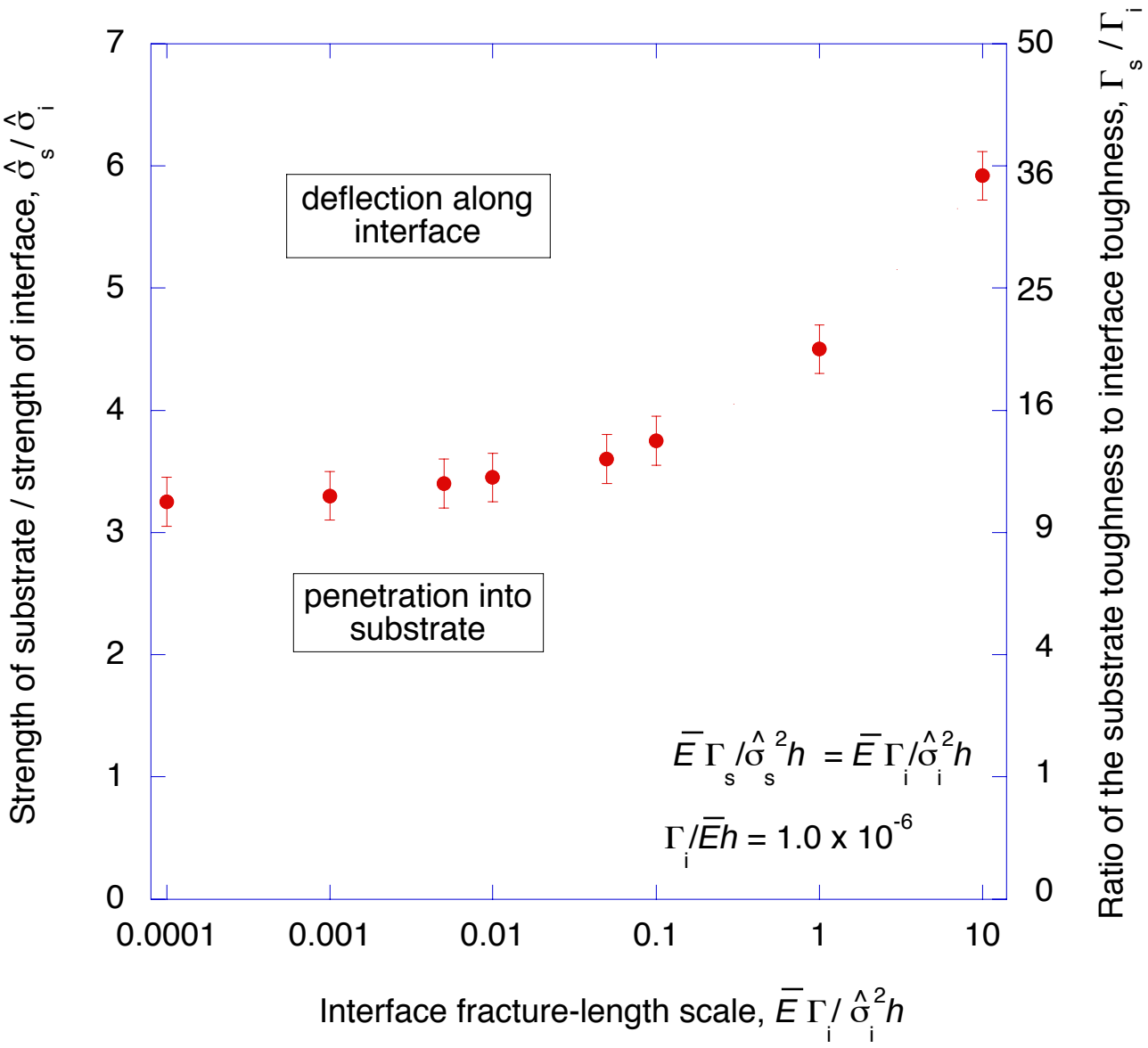
Strength of substrate / strength of interface, $\hat{\sigma}_s / \hat{\sigma}_i$
Ratio of the substrate toughness to interface toughness, Γ_s / Γ_i
Interface fracture-length scale, $\bar{E}\Gamma_i / \hat{\sigma}_i^2 h$
deflection along interface
penetration into substrate
$\bar{E}\Gamma_s / \hat{\sigma}_s^2 h = \bar{E}\Gamma_i / \hat{\sigma}_i^2 h$
$\Gamma_i / \bar{E} h = 1.0 \times 10^{-6}$
0
1
2
3
4
5
6
7
0
1
4
9
16
25
36
50
0.0001
0.001
0.01
0.1
1
10

Figure 7

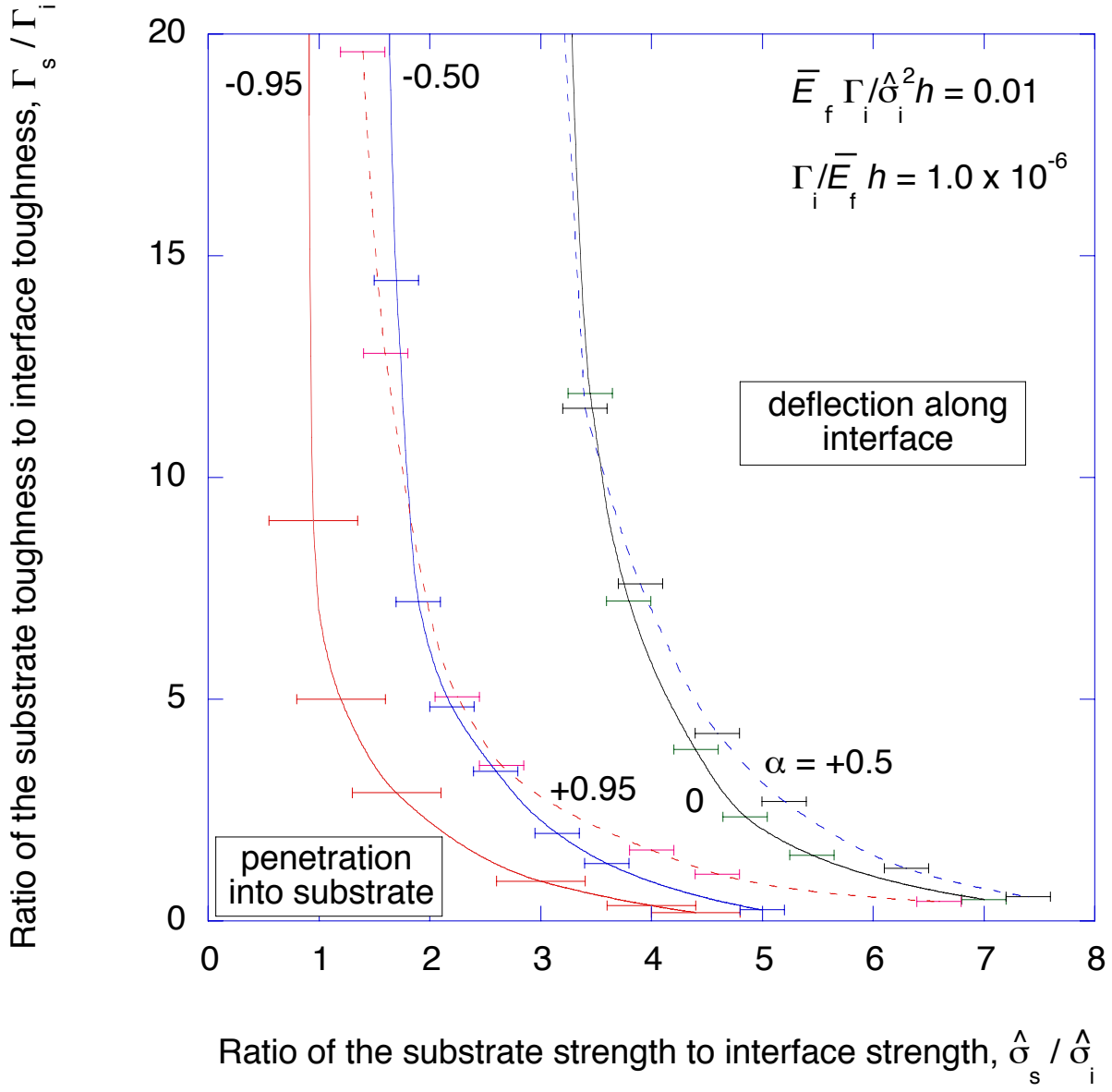
Ratio of the substrate toughness to interface toughness, Γ_s / Γ_i
Ratio of the substrate strength to interface strength, $\hat{\sigma}_s / \hat{\sigma}_i$
$\bar{E}_f \Gamma_i / \hat{\sigma}_i^2 h = 0.01$
$\Gamma_i / \bar{E}_f h = 1.0 \times 10^{-6}$
-0.95
-0.50
+0.95
0
α = +0.5
deflection along interface
penetration into substrate
0
5
10
15
20
0
1
2
3
4
5
6
7
8

Figure 8

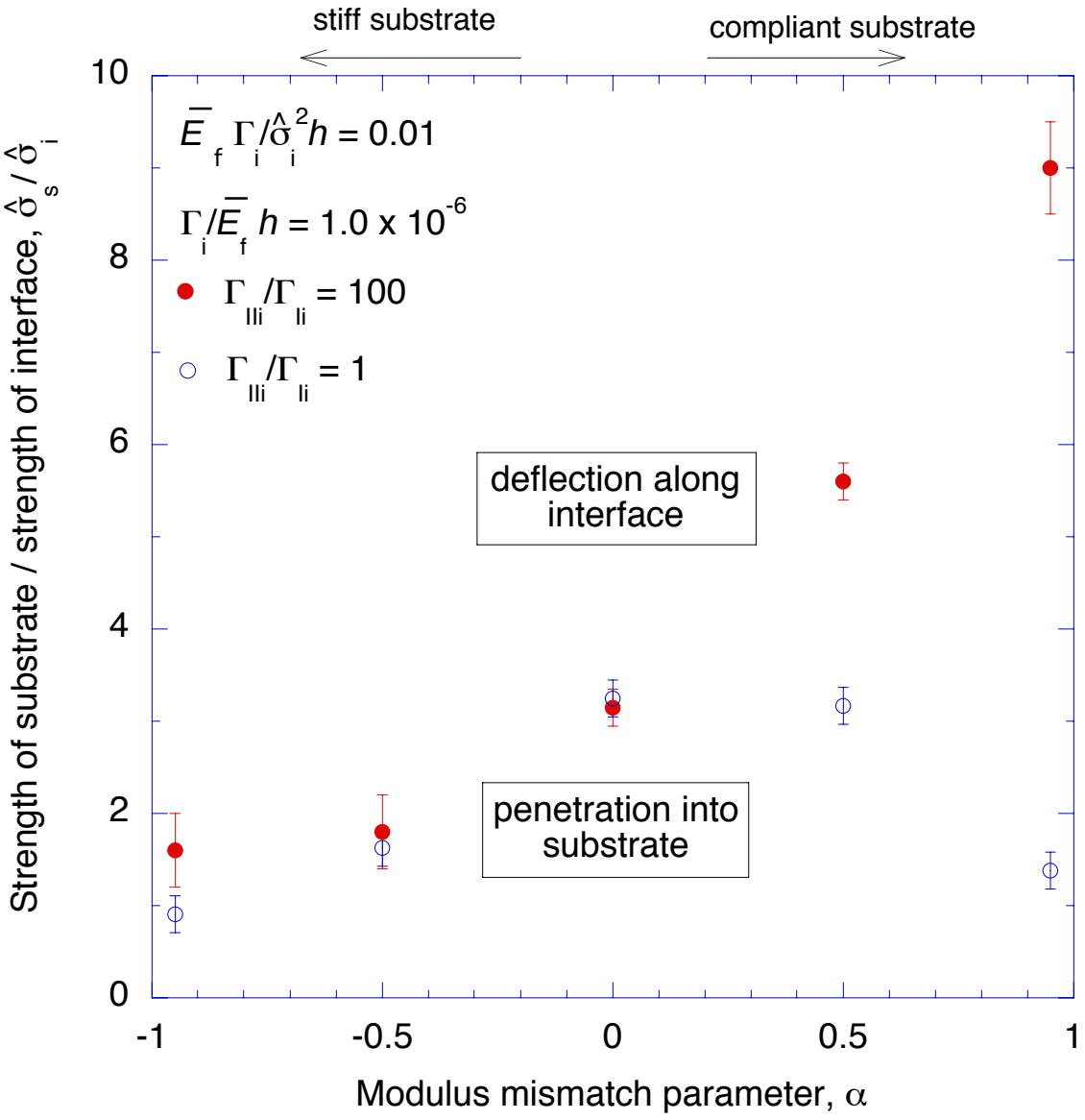
stiff substrate
compliant substrate
$\bar{E}_f \Gamma_i / \hat{\sigma}_i^2 h = 0.01$
$\Gamma_i / \bar{E}_f h = 1.0 \times 10^{-6}$
$\Gamma_{IIi} / \Gamma_{Ii} = 100$
$\Gamma_{IIi} / \Gamma_{Ii} = 1$
deflection along interface
penetration into substrate
Strength of substrate / strength of interface, $\hat{\sigma}_s / \hat{\sigma}_i$
Modulus mismatch parameter, α
10
8
6
4
2
0
-1
-0.5
0
0.5
1

Figure 9

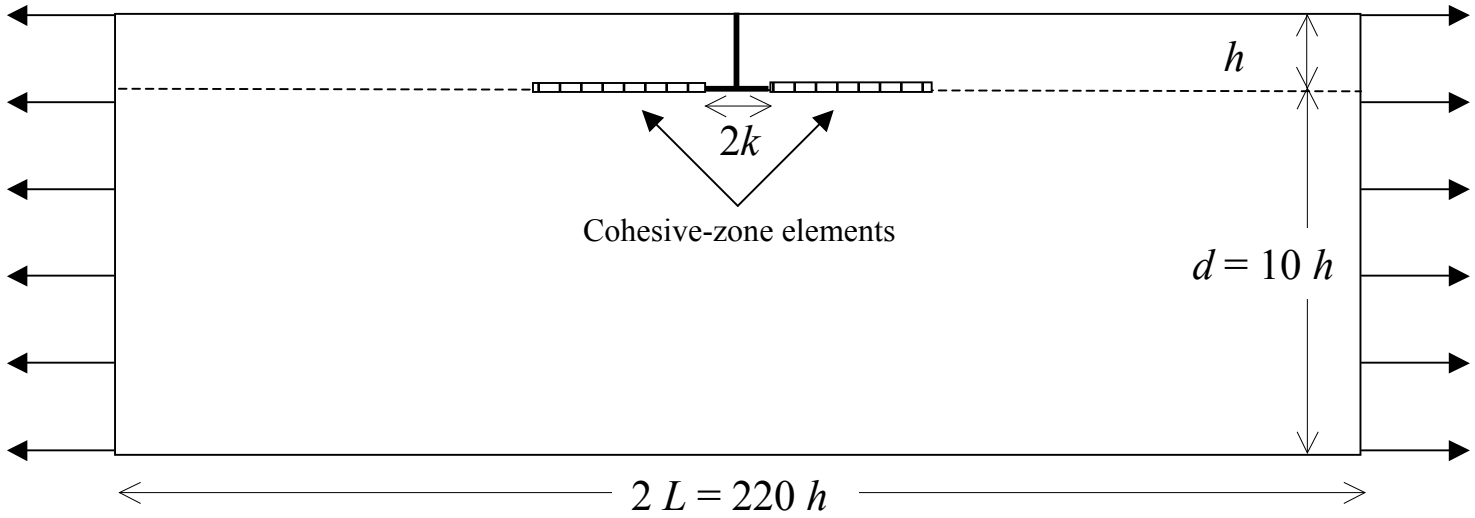
h
2k
Cohesive-zone elements
d = 10 h
2 L = 220 h

(a)

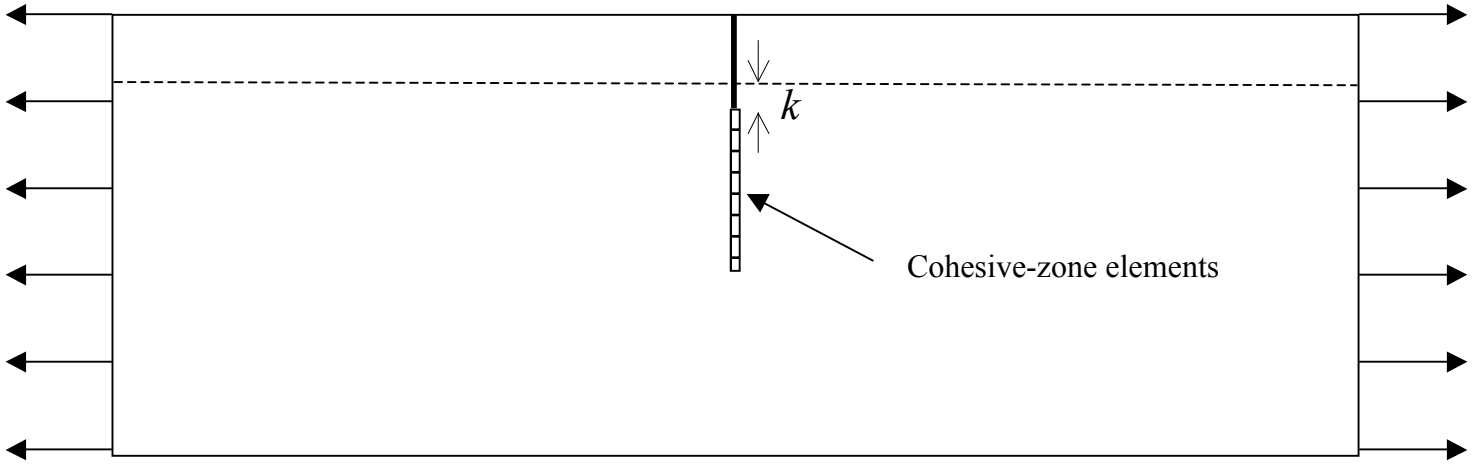
k
Cohesive-zone elements

(b)

Figure 10

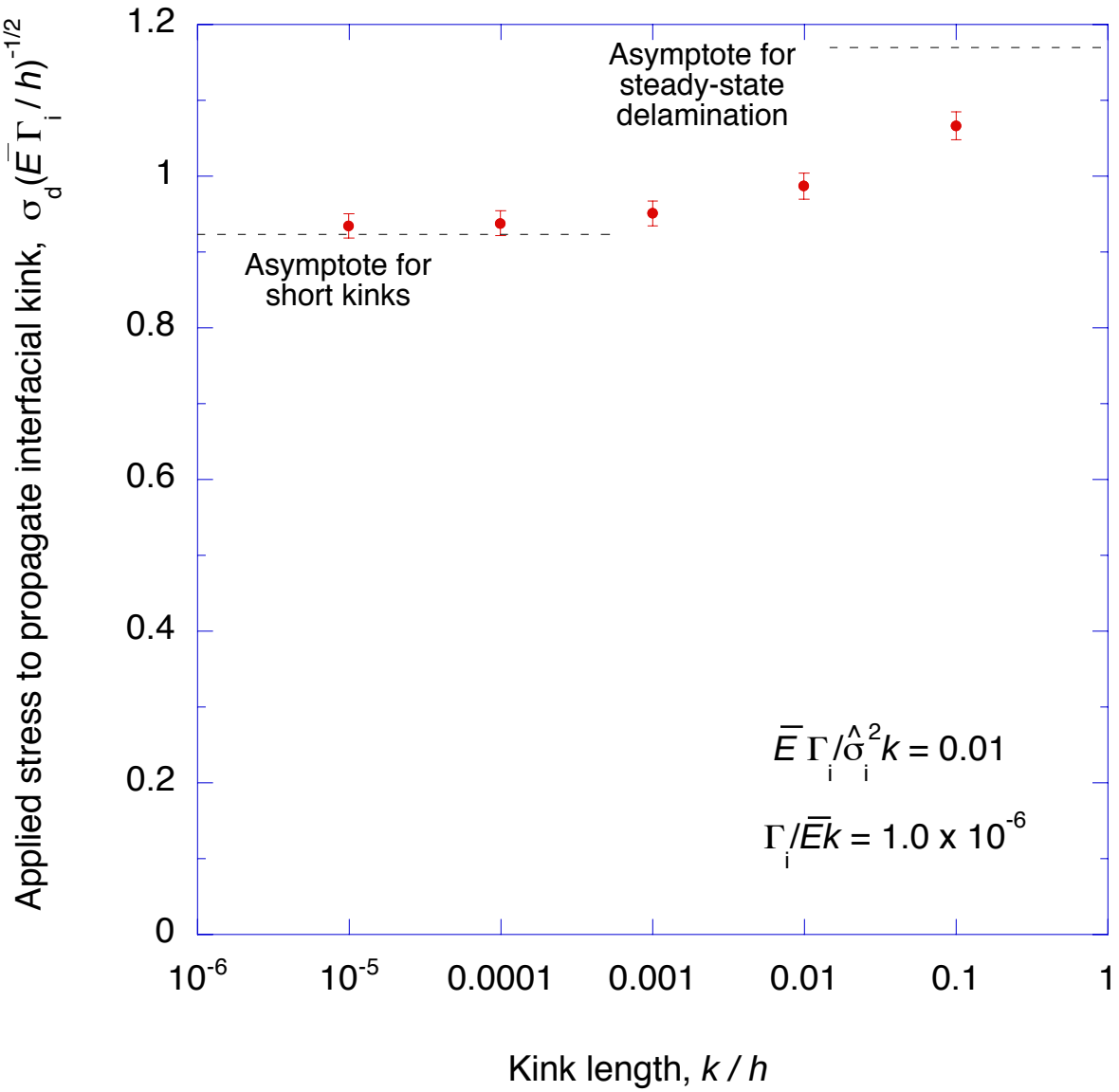
Applied stress to propagate interfacial kink, $\sigma_d(\bar{E}\Gamma_i / h)^{-1/2}$
1.2
1
0.8
0.6
0.4
0.2
0
Asymptote for steady-state delamination
Asymptote for short kinks
$\bar{E}\Gamma_i/\hat{\sigma}_i^2 k = 0.01$
$\Gamma_i/\bar{E}k = 1.0 \times 10^{-6}$
10^{-6}
10^{-5}
0.0001
0.001
0.01
0.1
1
Kink length, k / h

Figure 11

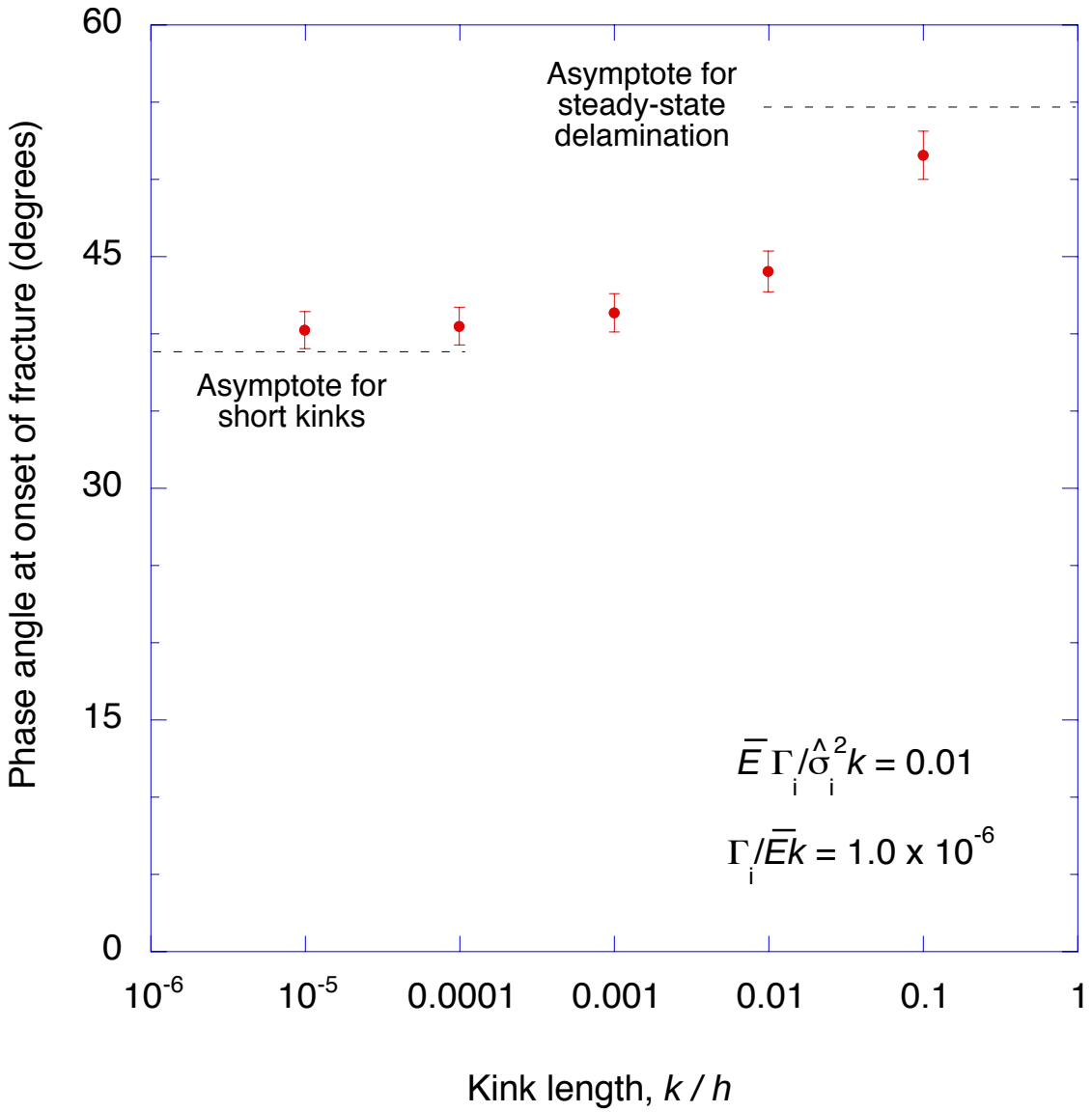
60
45
30
15
0
Phase angle at onset of fracture (degrees)
Asymptote for
steady-state
delamination
Asymptote for
short kinks
$\bar{E}\,\Gamma_i/\hat{\sigma}_i^2 k = 0.01$
$\Gamma_i/\bar{E}k = 1.0 \times 10^{-6}$
10^{-6}
10^{-5}
0.0001
0.001
0.01
0.1
1
Kink length, k / h

Figure 12

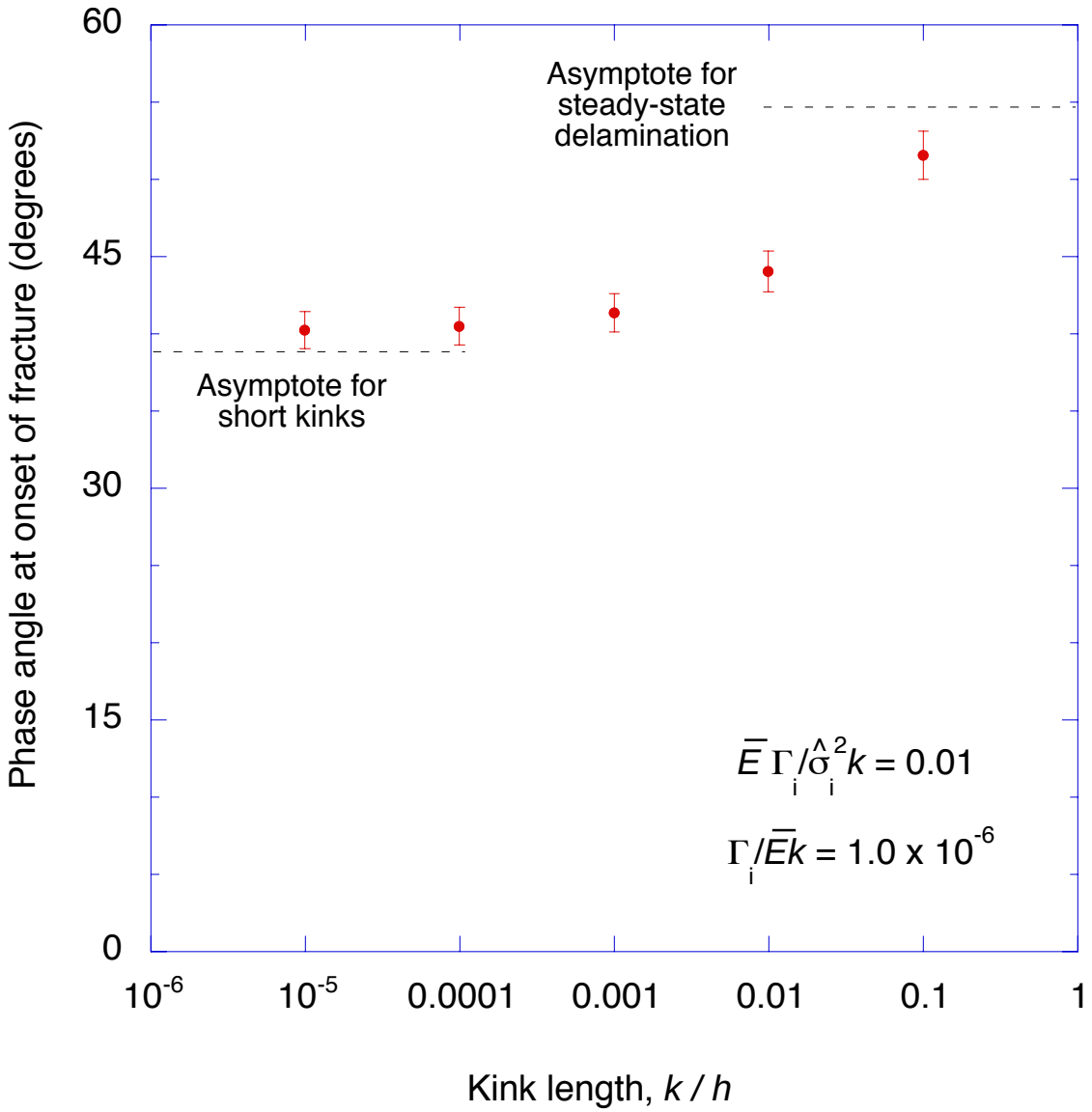
60
45
30
15
0
Phase angle at onset of fracture (degrees)
Asymptote for
steady-state
delamination
Asymptote for
short kinks
$\bar{E}\,\Gamma_i/\hat{\sigma}_i^2 k = 0.01$
$\Gamma_i/\bar{E}k = 1.0 \times 10^{-6}$
10^{-6}
10^{-5}
0.0001
0.001
0.01
0.1
1
Kink length, k / h

Figure 12

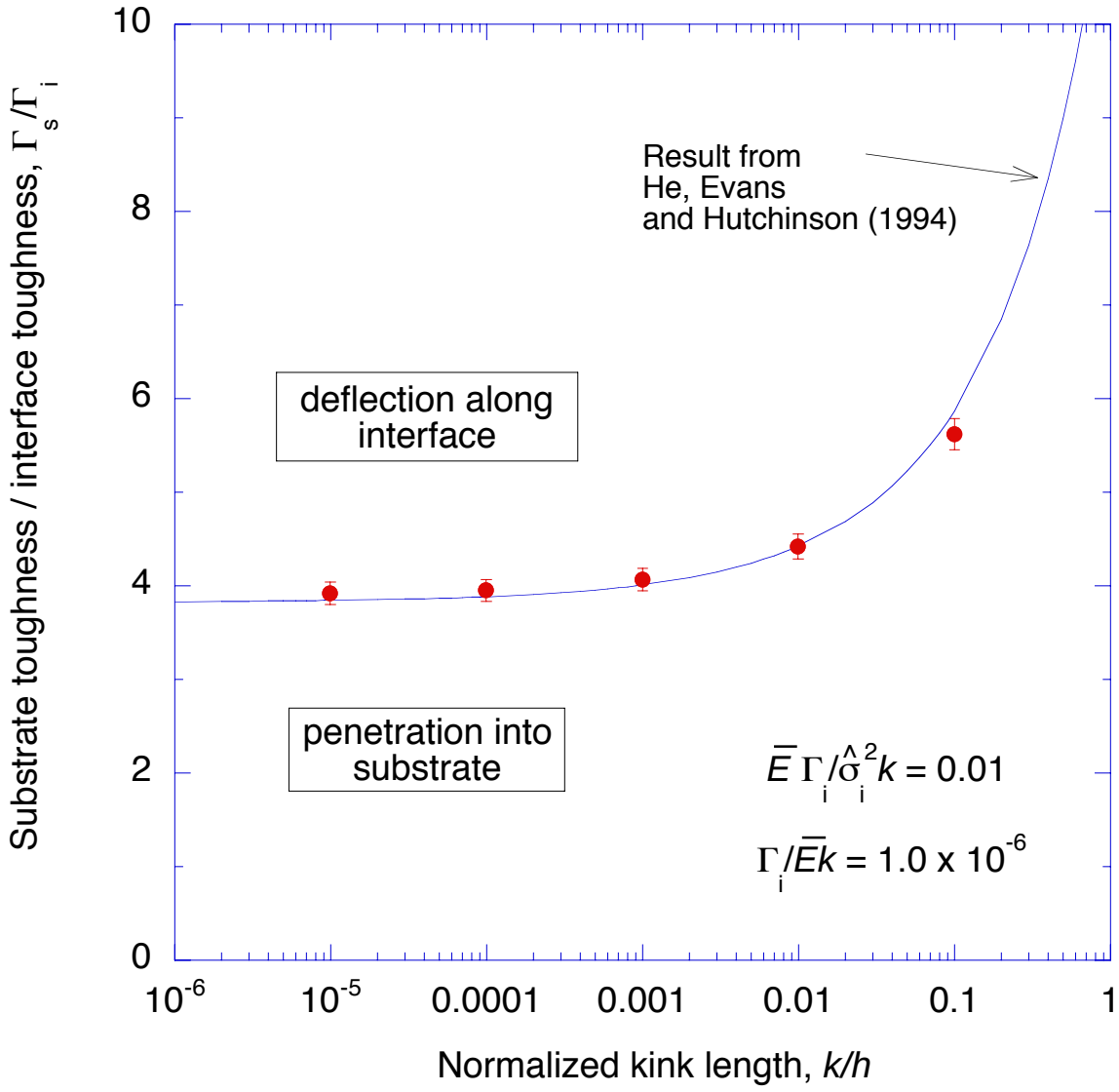
Substrate toughness / interface toughness, Γ_s/Γ_i
10
8
6
4
2
0
Result from
He, Evans
and Hutchinson (1994)
deflection along
interface
penetration into
substrate
$\bar{E}\,\Gamma_i/\hat{\sigma}_i^2 k = 0.01$
$\Gamma_i/\bar{E}k = 1.0 \times 10^{-6}$
10^{-6}
10^{-5}
0.0001
0.001
0.01
0.1
1
Normalized kink length, k/h

Figure 13